

SASSI-SRSS Approach for SSI Analysis with Incoherent Ground Motions

Farhang Ostadan

Nan Deng

**Bechtel National
San Francisco, CA**

August, 2007

~~©Bechtel Corporation 2007. This document contains proprietary information to Bechtel and its affiliated companies. The document is distributed to NEI and NRC and their consultants for the sole purpose of review/comment in support of new power plant licensing and should not be used for any other purposes.~~

F-1

PREFACE

The right, title and interest with the computer program SASSI remains with the Regents of the University of California, Berkeley. The licensing of the program is only permitted by the Regents and/or its authorized agents.

1. Introduction

This document presents the theoretical background on formulation of the ground motion incoherency models in the computer program SASSI2000 (Lysmer, et. al, 1999), a brief summary of the incoherency models implemented, computational steps to perform soil-structure interaction (SSI) analysis with incoherency models, and a summary of the verification of the new implemented feature. The general guide lines for using the incoherency option are described at the end.

2. Ground Motion Incoherency Models

Two incoherency models have been implemented in SASSI2000, the model by Mita and Luco (1986) and the model by Abrahamson (2006, 2007). In these models the lateral variability of the ground motion in the horizontal and vertical directions is characterized using the coherency function, $\gamma_{ij}(\omega)$, defined as

$$\gamma_{ij}(\omega) = \frac{S_{ij}(\omega)}{\sqrt{S_{ii}(\omega)S_{jj}(\omega)}} \quad (2.1)$$

where $S_{ii}(\omega)$ and $S_{jj}(\omega)$ are the auto power spectrum density functions (PSD) of the motions at locations i and j , and $S_{ij}(\omega)$ is the cross PSD between motions at locations i and j .

a. Mita and Luco's Model

This model is a theoretical model that defines the spatial coherence function by:

$$\gamma_{ij}(r, \omega) = \exp\{-[\gamma\omega |\vec{r}_j - \vec{r}_i| / V_s]^2\} \quad (2.2)$$

where γ is the dimensionless spatial incoherence parameter, V_s is the soil shear wave velocity and ω is the circular frequency (rad/sec).

The distance $|\vec{r}_j - \vec{r}_i|$ is the measure of separation of two points, i and j , in the ground. As shown in Equation (2.2), for short separation and low frequency, coherency function approaches one i.e., the effect of spatial variability is very small. As the separation distance and frequency increase, the coherency decreases (or incoherency increases).

This model is not expected to be used for design purposes. However, as discussed later, there are number of SSI analytical solutions published using the above model that permits verification of SSI formulation implemented in SASSI2000 with this model. The SSI computational steps remain the same among the models once the model type is selected for the analysis.

b. Abrahamson's Model

Abrahamson has updated his model incorporating the most recent data from dense arrays. His model provides the incoherency functions for soil sites for surface motion and motions within shallow depths and also a most recent model for rock sites. The models are all empirical and are based on a large set of recorded motions. The details of the model and its basis are documented in separate reports by Abrahamson (2006, 2007).

Following the analysis of large set of recordings, the model proposed for SSI analysis is the plane wave coherency model defined by the following functional form.

$$\gamma_{pw}(f, \xi) = \left[1 + \left(\frac{f \operatorname{Tanh}(a_3 \xi)}{a_1 f_c} \right)^{n_1} \right]^{-1/2} \left[1 + \left(\frac{f \operatorname{Tanh}(a_3 \xi)}{a_2 f_c} \right)^{n_2} \right]^{-1/2} \quad (2.3)$$

In the above equation, f is the frequency in Hz, ξ is the separation distance in meter (m). The coefficients for the model are provided by Abrahamson for soil sites for motions at ground surface and at shallow depths as well as for rock sites. Equation (2.3) provides the plane-wave coherency that should be used if a single plane wave is used as the input to the SSI model. The coherency functions for soil sites are plotted in Figure 2.1 for both horizontal and vertical directions for a range of separation distances. As depicted in this figure, the coherency decreases with increasing frequency and separation distance.

It should be noted the model represented by Equation (2.3) provides the functional relationships or constrains among the motions of a set of ground nodal points in the free-field in terms of auto and cross power spectral density functions in a normalized form. The actual intensity of the motion is defined by design motion and will be used in the analysis as described later while maintaining the constrains imposed by the model in terms of cross-power spectra density function.

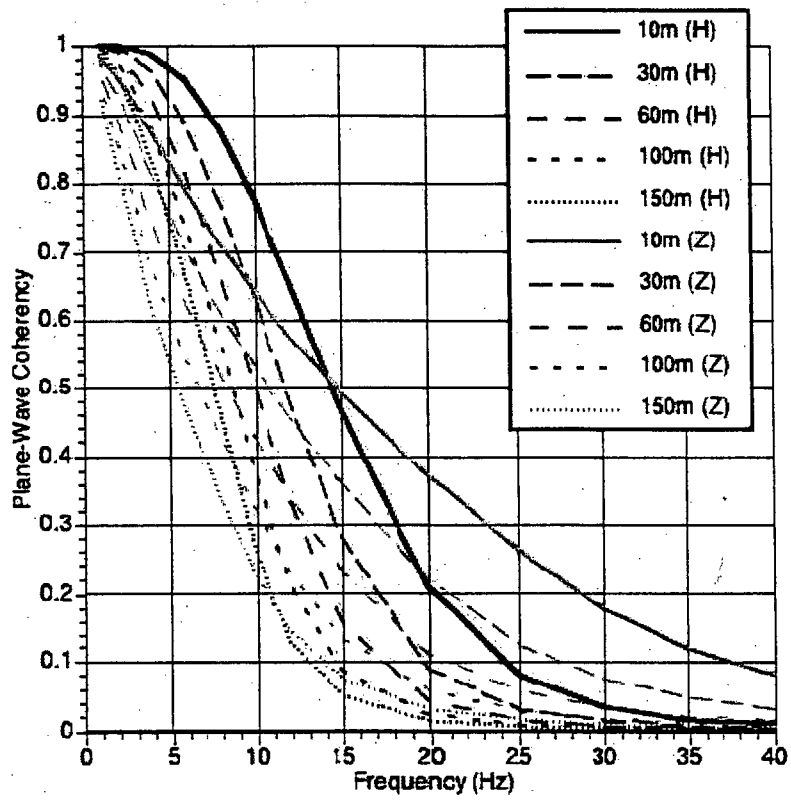


Figure 2.1. Horizontal and Vertical Components of the Plane-Wave Coherency Models.

3. Theoretical Formulation of Incoherency Computation in SASSI2000 Soil-Structure Interaction Framework

Seismic motions for “ m ” points in the ground at a given frequency ω can generally be characterized by the following power spectrum density (PSD) matrix

$$[S_g(\omega)] = \begin{bmatrix} S_{1,1}(\omega) & S_{1,2}(\omega) & \cdots & S_{1,m}(\omega) \\ S_{2,1}(\omega) & S_{2,2}(\omega) & \cdots & S_{2,m}(\omega) \\ \vdots & \vdots & S_{i,j}(\omega) & \vdots \\ S_{m,1}(\omega) & S_{m,2}(\omega) & \cdots & S_{m,m}(\omega) \end{bmatrix} \quad (3.1)$$

In this matrix, the diagonal terms $S_{i,i}(\omega)$ are the auto power spectral density (PSD) function for motion at location i , and $S_{i,j}(\omega)$ are the cross PSD functions between motions at locations i and j . $[S_g(\omega)]$ is by definition a hermitian matrix, i.e., $[S_g(\omega)]^* = [S_g(\omega)]$, and $S_{j,i}(\omega) = \overline{S_{i,j}(\omega)}$, where the “*” denotes conjugated transpose, and the top bar, “-”, denotes conjugate of the complex term. Therefore the diagonal terms, $S_{i,i}(\omega)$, $i=1, \dots, m$, are positive real functions.

It should be noted that the coherency models and the associated PSD matrix only provide the amplitudes of PSD functions of the ground motions in a normalized form. These functions do not provide any information on the relative phasing of the motions among the group of “ m ” nodes. Thus, application of this model to structural analysis stipulates a formulation that is capable of obtaining the PSD of the structural response accurately. Similarly for SSI analysis, the approach adopted in SASSI2000 is such that it amounts to the PSD of the response quantity of interest consistent with the nature of the input motion expressed by PSD functions. As shown below the square root of sum of the squares (SRSS) summation on spatial modal structural responses is the preferred method that solves for the accurate PSD of the structural responses.

Given the property of the PSD matrix described above, the matrix can be written in the following form

$$[S_g(\omega)] = [S_D][\Gamma(\omega)][S_D] \quad (3.2)$$

Where

$$[S_D] = \text{diag}[\sqrt{S_{1,1}}, \sqrt{S_{2,2}}, \dots, \sqrt{S_{m,m}}] \quad (3.3)$$

$$[\Gamma(\omega)] = \begin{bmatrix} 1 & \gamma_{1,2} & \cdots & \gamma_{1,m} \\ \gamma_{2,1} & 1 & \cdots & \gamma_{2,m} \\ \vdots & \vdots & \ddots & \vdots \\ \gamma_{m,1} & \gamma_{m,2} & \cdots & 1 \end{bmatrix} \quad (3.4)$$

$$\gamma_{i,j}(\omega) = \frac{S_{i,j}}{\sqrt{S_{i,i} \cdot S_{j,j}}} \quad (3.5)$$

γ_{ij} is the coherency function, such as the relationships developed by Mita and Luco (Equation 2.2) or by Abrahamson (Equation 2.3). By definition γ_{ij} is a positive real function. However, a complex phase factor may be applied on γ_{ij} to reflect the effect of traveling waves. In the following discussion it is assumed that the general complex form is utilized.

The PSD matrix $[S_g(\omega)]$ can be expressed in the following form:

$$[S_g(\omega)] = \sum_{i=1}^m \lambda_i \{\phi\}_i \{\phi\}_i^* \quad (3.6)$$

Where λ_i and $\{\phi\}_i$ are the eigenvalues and eigenvectors of the matrix that satisfy the relationships

$$[S_g(\omega)] \{\phi\}_i = \lambda_i \{\phi\}_i, \quad i = 1, \dots, m; \quad (3.7)$$

λ_i are all real numbers while $\{\phi\}_i$ are in general complex vectors satisfying

$$\{\phi\}_i^* \cdot \{\phi\}_j = \delta_{i,j} = \begin{cases} 1, & i = j \\ 0 & i \neq j \end{cases} \quad (3.8)$$

Equation (3.7) shows that for “ m ” number of nodes in the ground, a set of “ m ” eigen vectors (mode shapes) and associated eigen values can be obtained from the PSD matrix. These modes can in fact be plotted. The main modes show modal shapes associated with rigid body motion of the group of “ m ” nodes whereas the higher modes depict the rotations and deformed shape of the group.

Implementation of the incoherency model in SASSI2000 follows its sub-structuring method. The commonly used sub-structuring formulations of the SSI problem for a fully coherent wave field are presented in Attachment A. As shown in this Attachment, the equation of motion for SASSI2000 “subtraction method” for each frequency requires computation of the vector U'_f representing the free-field motion for all interaction nodes (Equation A.3-3). In a deterministic fully coherent analysis, U'_f is obtained from the solution to the site response problem in layered media and depends on the wave type and

layered properties. U'_f is a vector normalized to the amplitude of motion at the control point using harmonic motion with unit amplitude at the control point. For incoherency analysis, U'_f can be expressed in terms of the eigen vectors and eigen values shown in Equation (3.7).

In the following section it is shown that once the solution of the structural response subjected to the individual mode and associated eigen value is obtained, the SRSS of solutions for all the modes results in an accurate expression of the PSD of the structural responses consistent with the prescribed PSD of the input motion.

The total responses of the structure system can be obtained by solving the equation of motion to each of the eigen-pairs, i.e., construct the modal ground motion vector $\{u_g\}_j$

$$\{u_g\}_j = \sqrt{\lambda_j} \{\phi\}_j, j = 1, \dots, m \quad (3.9)$$

and solving the equation of motion (Equation A.3-3). Assuming a surface foundation for the sake of simplicity in the derivation, the SASSI Equations of Motion can be written as

$$\begin{bmatrix} C_{ii} + X_{ii} & C_{is} \\ C_{si} & C_{ss} \end{bmatrix} \begin{Bmatrix} u_i \\ u_s \end{Bmatrix}_j = \begin{Bmatrix} X_{ii} u_{g,j} \\ 0 \end{Bmatrix} \quad (3.10)$$

where the subscript i denotes the interaction nodes, and the subscript s is for all structural nodes (see Attachment A). X_{ii} is the impedance matrix of dimension $m \times m$. Let $\{u\} = \{u_i, u_s\}^T$, the solution of Equation (3.10) leads to

$$\{u\}_j = [H] \{u_g\}_j \quad (3.11)$$

where $[H] = [H_i, H_s]^T$, is the transfer function matrix, $[H]$ is of dimension $n \times m$. The components of $[H]$ are of the following form

$$H_i = [C_{ii} + X_{ii} - C_{is} C_{ss}^{-1} C_{si}]^{-1} X_{ii} \quad (3.12)$$

$$H_s = -C_{ss}^{-1} C_{si} H_i \quad (3.13)$$

After obtaining the solutions, $\{u\}_j, j = 1, \dots, m$, the PSD matrix of the responses of the structure system can then be obtained

$$[S_u(\omega)] = \sum_{j=1}^m \{u\}_j \{u\}_j^* \quad (3.14)$$

Equation (3.14) can be proved easily. In fact, from Equations (3.6), (3.9), (3.11), it can be shown that

$$\sum_{j=1}^m \{u\}_j \{u\}_j^* = \sum_{j=1}^m [H] \{u_g\}_j \{u_g\}_j^* [H]^* = [H] \left(\sum_{j=1}^m \lambda_j \{\phi\}_j \{\phi\}_j^* \right) [H]^* = [H][S_g][H]^* \quad (3.15)$$

Note the diagonal terms of $[S_u]$, e.g., the k -th diagonal term, or the auto PSD for k -th DOF:

$$S_{u,kk} = \sum_{j=1}^m u_{k,j} \overline{u_{k,j}} = \sum_{j=1}^m |u_{k,j}|^2 \quad (3.16)$$

where $u_{k,j}$ is the k -th term of the solution vector $\{u\}_j$. Note the summation is through all spatial eigen modes.

Equation (3.16) shows that the auto PSD of any degree-of-freedom (DOF) in the structure system can be obtained by first solving the equations of motion for all eigen modes of the incoherent ground motion model obtained from the PSD matrix, then sum up the square of the amplitudes of the response from the solutions of all modes.

The above discussion outlines the general approach in solving the SSI problem and obtaining PSDs at all nodal points with the ground motion incoherency PSD matrix defined. The method permits use of different motions at the m support points, i.e., the diagonal terms in $[S_g]$, $S_{1,1}$, $S_{2,2}$, ..., $S_{m,m}$, can all be different. However, in most practical applications, the ground motion is defined by a single design motion and the PSD of the ground motions at all nodes are the same as the PSD of the design motion. This is a reasonable assumption given the typical size of the foundations for critical facilities. Let S_0 be the uniform PSD for all nodes,

$$S_{1,1} = S_{2,2} = \dots = S_{m,m} = S_0 \quad (3.17)$$

And Equation (3.2) reduces to

$$[S_g] = [\Gamma] \cdot S_0 \quad (3.18)$$

Note that S_0 is a single number for each frequency and can be taken out of the matrix operations. We can perform the eigen-decomposition and solution steps on $[\Gamma]$ only and multiply S_0 back at the last step. Following Equation (3.16) and the above assumption, the auto PSD of motion at the k -th DOF can be written as

$$S_{u,kk} = \left(\sum_{j=1}^m |u_{k,j}|^2 \right) \cdot S_0 \quad (3.19)$$

Recall from the basic stochastic theory that for a linear system, the PSD of the system response, S_{out} , can be represented as the product of the PSD of input, S_{in} , and the square of the amplitude of the transfer function H , i.e.,

$$S_{out}(\omega) = |H(\omega)|^2 \cdot S_{in}(\omega) \quad (3.20)$$

Comparing Equations (3.19) and (3.20), it is concluded that the total response of the structure in terms of amplitude of transfer functions at any DOF can be calculated as the SRSS of all spatial modal solutions.

$$|H(\omega)|_k = \sqrt{\sum_{j=1}^m |u_{j,k}|^2} \quad (3.21)$$

It should be noted that the above derivation provides the exact solution for the linear system since there is no other assumption/simplification introduced in the solution process.

This approach is equally applicable to the calculation of structure forces and stresses due to the incoherent ground motion. Let $[K_e]$ be the element stiffness matrix. After solving Equation (3.10) and obtaining the modal displacement solutions $\{u\}_j$, the corresponding modal force solution $\{f\}_j$ can be obtained by (conversion from global coordinates to local coordinates is implied)

$$\{f\}_j = [K_e]\{u\}_j \quad (3.22)$$

Similarly, amplitude of the force/stress transfer function at any DOF k can be obtained as

$$|Q(\omega)|_k = \sqrt{\sum_{j=1}^m |f_{j,k}|^2} \quad (3.23)$$

In summary the above derivation confirms that, for ground motion incoherency models formulated by the PSD matrix, the SRSS summation on spatial modal solutions is an accurate method to compute the structural responses and is consistent with development of the PSD of structural response subjected to the incoherent ground motions models characterized by the PSD functions. A rational extension of this method is incorporation of the random vibration theory (RVT) in the formulation of the SSI solution. RVT approach can be directly implemented so that by providing the response spectra or PSD of input motion, the structural responses in terms of the power or response spectra can be readily computed.

Estimate of Truncation Errors

Equation (3.16) establishes the exact solution form for the auto PSD at any specified DOF. Furthermore, Equation (3.21) gives the equivalent transfer function for the DOF if the ground motions at all interaction nodes are specified by the same PSD value, S_0 . A complete solution, however, is quite time consuming since it would require that the equations of motion, Equation (3.10), be solved for all m spatial modes. In engineering practice, however, only a subset of these spatial modes needs to be solved to obtain satisfactory solutions. The following section establishes an estimate on the upper bound

of potential truncation errors of the solution by using only a subset of the eigen-mode solutions.

The following characteristics of the solutions are observed from Equations (3.9), (3.11) and (3.16):

- (1) For each spatial mode, the magnitude of the solution vector is directly proportional to the magnitude of the corresponding eigenvalue. In fact,

$$\{u\}_j = [H]\{u_g\}_j = [H]\sqrt{\lambda_j}\{\phi\}_j \quad j = 1, 2, \dots, m \quad (3.24)$$

$$|\{u_j\}|^2 = \{u_j\}^* \{u_j\} = \sum_{k=1}^n \overline{u_{k,j}} \cdot u_{k,j} = |\lambda_j| \cdot \|\{\phi\}_j^* [H]^* [H] \{\phi\}_j\| = |\lambda_j| \cdot C_j \quad (3.25)$$

where “*” denotes for conjugated transpose, $\|\{\phi\}_j^* [H]^* [H] \{\phi\}_j\|$ is the absolute value of the determinant of a square matrix, and C_j is that value. It can be proved that for all spatial modes, $j = 1, 2, \dots, m$, $C_1 = C_2 = \dots = C_m = C$ since $[H]$ is independent to the ground motions, and all $\{\phi\}_j$ are unit vectors.

- (2) Following Equation (3.25), the square sum of the overall solution is directly proportional to the sum of the absolute value of the eigenvalues. i.e.,

$$\sum_{j=1}^m |\{u_j\}|^2 = \left(\sum_{j=1}^m |\lambda_j| \right) \cdot C \quad (3.26)$$

Equation (3.26) indicates that contributions of all spatial modes to the overall solutions are additive since the right-hand-side in (3.26) are positive for all j values. Thus, if we rearrange all eigenvalues from the largest to the smallest, and use a subset of only the first “ s ” eigen-solutions, $s \ll m$, the truncation error of this subset can be established as:

$$|\varepsilon|_s = \frac{1 - \sqrt{\sum_{j=1}^s |u_j|^2}}{\sqrt{\sum_{j=1}^m |u_j|^2}} = \frac{1 - \sqrt{\sum_{j=1}^s |\lambda_j|}}{\sqrt{\sum_{j=1}^m |\lambda_j|}} \quad s \ll m \quad (3.27)$$

Equation (3.27) establishes the upper bound of truncation errors for the computation of the transfer functions as defined by Equation (3.21) since this estimate is for the magnitude of the entire PSD matrix and the solutions from Equation (3.21) is only a subset of the PSD solutions. This estimate is also easy to implement in practical computations since all it requires is the ratio of two sums for the eigenvalues computed in the orthogonal decomposition process of the coherency matrix.

For most applications, it has been noted that using 10 spatial modes will result in accurate results with very small error. In the verification examples presented in Section 6, the errors due to selection of limited spatial modes have been computed and sensitivity of the results to limited number of spatial modes is demonstrated.

Frequencies of Analysis

For conventional SSI analysis, as described in SASSI user manual, a select group of 20 to 50 frequencies are sufficient to compute the total response of the structure. The results for the remaining frequencies are obtained using the interpolation scheme in SASSI which is based on the generalized shape of the transfer function for a two degree-of-freedom system. For application with incoherent motion, it should be noted that the incoherent ground motion is random in nature and the randomness is more evident at high frequencies. This effect causes additional rocking and torsional vibration of the structures. These modes of vibration can not be detected from conventional fixed base and SSI analysis of the structure. It is recommended that a larger set of frequency points to be used to capture additional modes of structural vibrations more accurately. Number of frequencies between 50 to 100 points is expected to be adequate. The solution for the remaining frequencies will be obtained using the same interpolation scheme implemented in SASSI since once the SRSS is performed on the spatial modal solutions, the results are the structural transfer functions independent of ground motions and can be interpolated as in the case of coherent ground motions.. It has been noted that performing interpolation on individual spatial modal solution would require careful examination and further smoothing of the interpolated results. This is mainly due to the fact that solution to each spatial mode is not the complete transfer function to represent the structural response and exhibits a significant undulation. The SRSS of the transfer function at computed frequencies provides the total structural response which is a much smoother response and can be used readily with the current SASSI interpolation scheme to obtain the transfer function for all other frequencies.

4. Implementation in the Computer Program SASSI2000

As shown in Equation (A.3-3), only the free-field load vector U'_f needs to be computed using the coherent or incoherent ground motion model. This vector is computed for each frequency and for the interaction nodes in contact with soil in the SSI model. To do so, the following steps are taken:

- For each frequency, the coherency functions in Equations (2.2) or (2.3) are used to construct the coherency matrix for all interaction nodes, i . The matrix can be readily constructed given the frequency of analysis and the separation distances among the nodes. This is a full matrix with off-diagonal terms reducing in absolute values as the separation distance among the nodes increases. Separate coherency matrices for horizontal and vertical motions are constructed.
- Each matrix is solved using a complex eigen equation solver to obtain the eigen values and eigen vectors. Eigen vectors are used as mode shapes. Modal weights are the square root of the eigen values. All or selected sets of modes can be considered in the analysis.
- The structural responses are computed for each spatial mode (Equation (3.9) provides successive ground motion vector U'_f). For embedded structures, the free-field vector is adjusted for amplitude reduction of free-field vector with depth just as it has been performed in the basic SASSI operation.
- The total responses, or the transfer functions (TF) of the structure, are obtained using the SRSS method combining all spatial modal solutions.
- Once the TF function for the response location of interest is obtained, other responses of interest such as time histories, response spectra, etc. follows the normal procedure using the Fourier Transform to convolve with the control motion.

5. User Guide for the Incoherency Option in SASSI20000

The user guide and technical manuals of the computer program SASSI2000 (Lysmer, et al, 1999) has been modified to include the incoherency models and the guide for its execution. The program has been modified in a manner to reduce the impact on input files previously generated for SSI analysis.

The revised layout of the program is shown in Figure 5.1. The sequence of runs and modeling guides can be summarized as follows.

- The free-field soil profile and choice of frequency of analysis are modeled using the program SITE with no change. The results of analysis are saved on Tapes 1 and 2 for the follow up runs.
- The program POINT remains the same and provides the point load solution to compute the impedance matrix.
- The program HOUSE also remains the same to model the finite element part of the SSI model.
- The new program INCOH has been developed to handle the incoherency models. This program reads the frequency points from Tape 1 (generated by SITE) and the nodal coordinate data from Tape 7 (generated by HOUSE). The program computes the coherency matrix and decomposes the matrix to obtain the eigen values and eigen vectors for each frequency of analysis. The results are saved on Tape 11.
- The program ANALYS has been modified to read the eigen values and eigen vectors from Tape 11 and solves for each mode. The results are saved on a series of Tapes 8 each containing the solution for the selected incoherency modes.
- The program COMBIN has been modified to perform SRSS on the modal solutions obtained from Tapes 8's and generate one final tape for the TF of the structure.
- The program MOTION remains the same and receives the TF from Tape 8 to compute other responses of interest (time histories, response spectra,...).

The general guidelines remain the same as those provided in SASSI2000 user manual. For incoherency analysis, the following needs to be observed.

- The incoherent ground motion is random in nature and the randomness is more evident at high frequency. This effect causes additional rocking and torsional vibration of the structures. These modes of vibration can not be detected from conventional fixed bases analysis and conventional SSI analysis of the structure. It is recommended that a larger set of frequency points to be used to capture additional modes of structural vibrations more accurately. Number of frequencies between 50 to 100 points is expected to be adequate.
- The spatial modes used in the analysis can be selected by the user. While user has the choice to use all the modes, it has been found that for critical structures with fairly rigid mat a few modes are adequate. For low frequency responses, 3 to 5

modes are capable of capturing the responses adequately. For higher frequency responses, a larger set of modes are needed. Analysis of typical nuclear power plants and comparison with other published solutions confirm that 10 spatial modes are generally adequate to obtain accurate results. The user has the option to increase the number of modes to ensure the responses are not impacted.

- Foundations, typically mat foundation, used for critical facilities are rigid in horizontal directions. The mat foundation is not necessarily rigid in vertical direction, particularly for high frequency responses. Due to spatial variability of the ground motion and additional rocking caused by vertical excitation, care must be exercised in modeling the mat foundation and its connection with interior and exterior walls to adequately capture the foundation flexibility effects. Assumption of rigid mat foundation for vertical analysis may not result in realistic responses of the structure.
- The spatial variability of incoherent ground motions is random in nature. No symmetry should be expected for the ground motions. Therefore, half or quarter SASSI models with symmetry planes should not be used.
- For the same reasons stated above, 2D SSI analysis should not be performed with the ground motion incoherency models

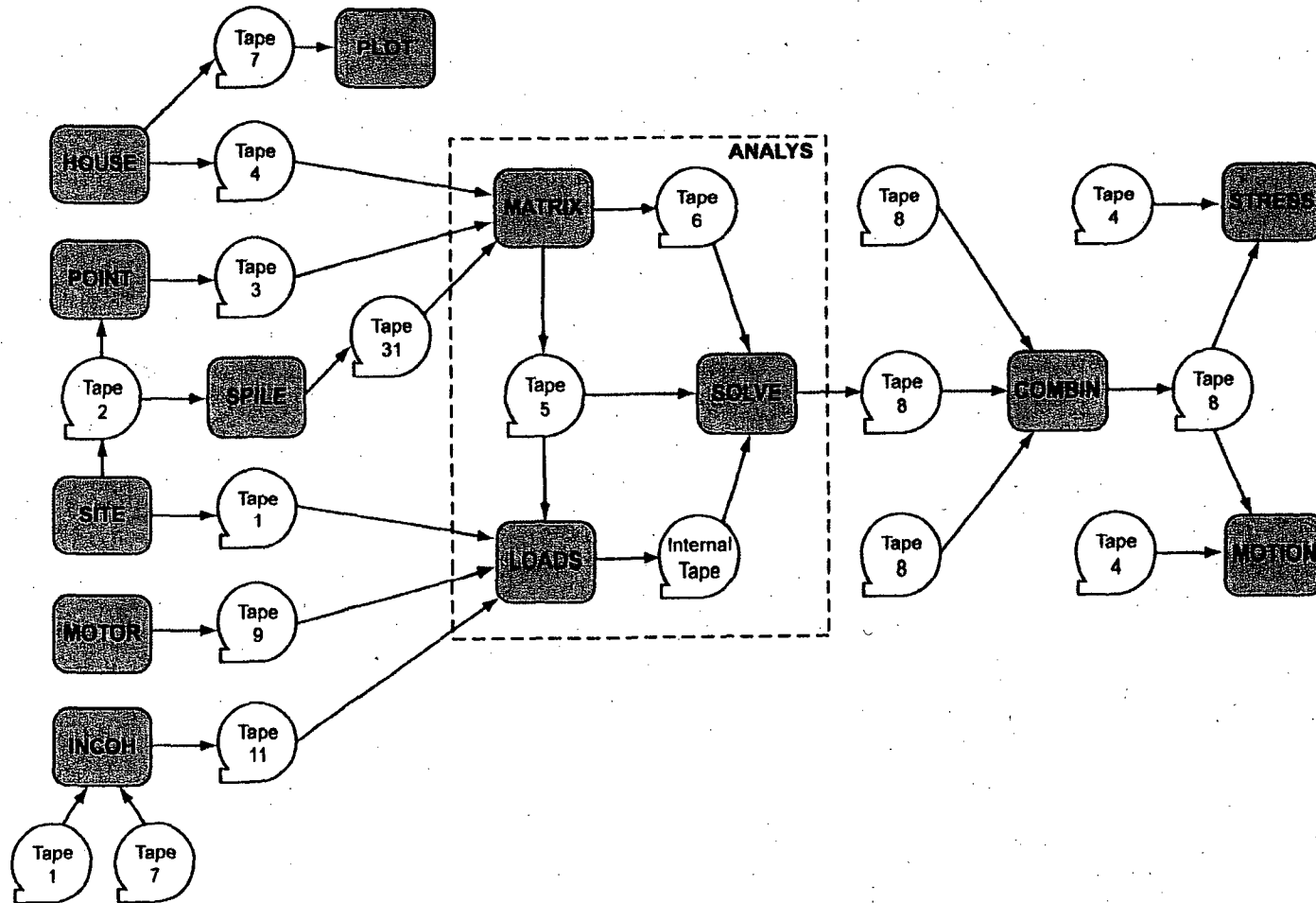


Figure 5.1 SASSI2000 Layout with Incoherency Feature

6. Verification of the SRSS Method for SSI Analysis with Incoherent Ground Motion

This section briefly presents the example problems used to verify the SRSS method for analyzing the incoherent ground motion. There are number of published SSI solutions using the theoretical model by Mita and Luco (1986). Since the same computational steps described in Section 3 are used, these example problems have been analyzed to verify accuracy of the solution. Sensitivity analyses are performed for the examples to illustrate the adequacy of using only limited spatial modes.

Example 1

Luco and Mita (1987) published analytical results for the responses of a rigid massless foundation on a homogeneous half-space subjected to incoherent ground motions defined by the Equation (2.1). The solutions for $\gamma = 0.1, 0.3$ and 0.5 are provided in tabulated form.

This problem is analyzed using SASSI2000. Results of analyses in terms of transfer functions in horizontal, vertical, rocking and torsional directions are compared with the Luco and Mita results (Figures 6.1, 6.3, 6.5, 6.7). SASSI numerical model for this problem has a total of 69 interaction nodes, thus a total of 69 spatial modes may be utilized in calculating the incoherent responses. All results shown above are computed using all 69 modes. As shown in the figures, agreement between these two sets of results is excellent.

A sensitivity analysis is performed on the effects of using a limited number of spatial modes. This sensitivity study is performed for the $\gamma = 0.5$ case only. Figures 6.2, 6.4, 6.6 and 6.8 show the truncation errors of the transfer functions if the SRSS combinations are performed using 10, 20 or 40 modes only. As shown in the figures, if 10 spatial modes are utilized, the maximum relative errors are less than 2% in the translational directions, and are less than 4% in the rotational directions. These numbers are considered very small considering the usual uncertainty involved in the dynamic calculations.

Figure 6.1
Horizontal Transfer Functions at Center of a Massless Circular Foundation
Incoherent Runs

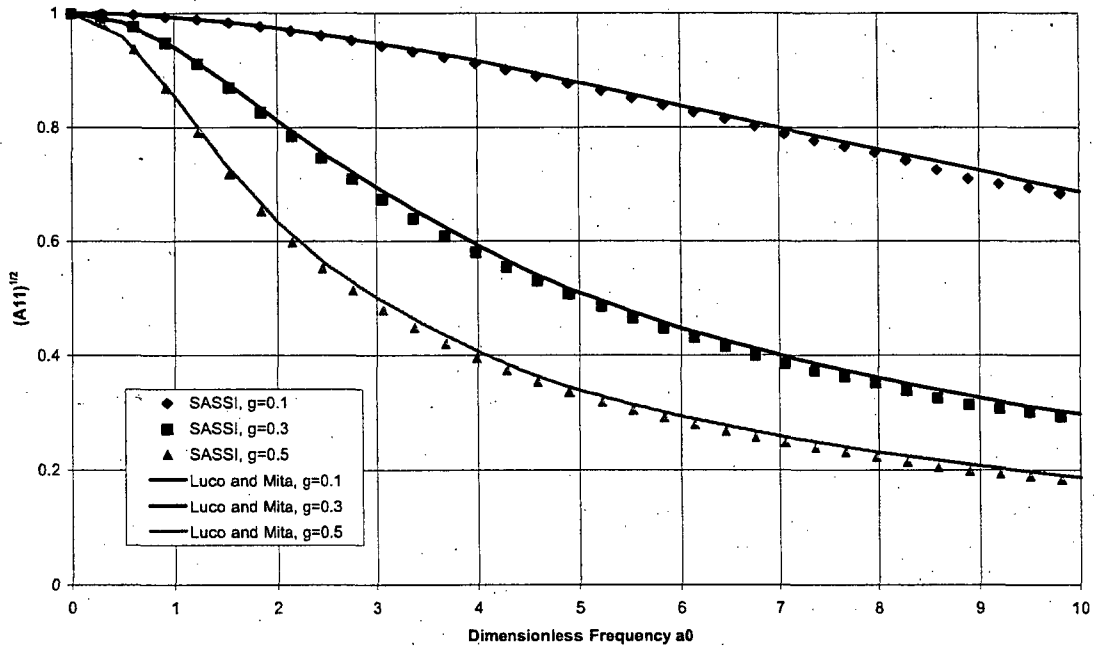


Figure 6.2
Truncation Errors Using Limited Spatial Modal Solutions
Horizontal Transfer Functions. At Center of Rigid Massless Disk, $\gamma = 0.5$

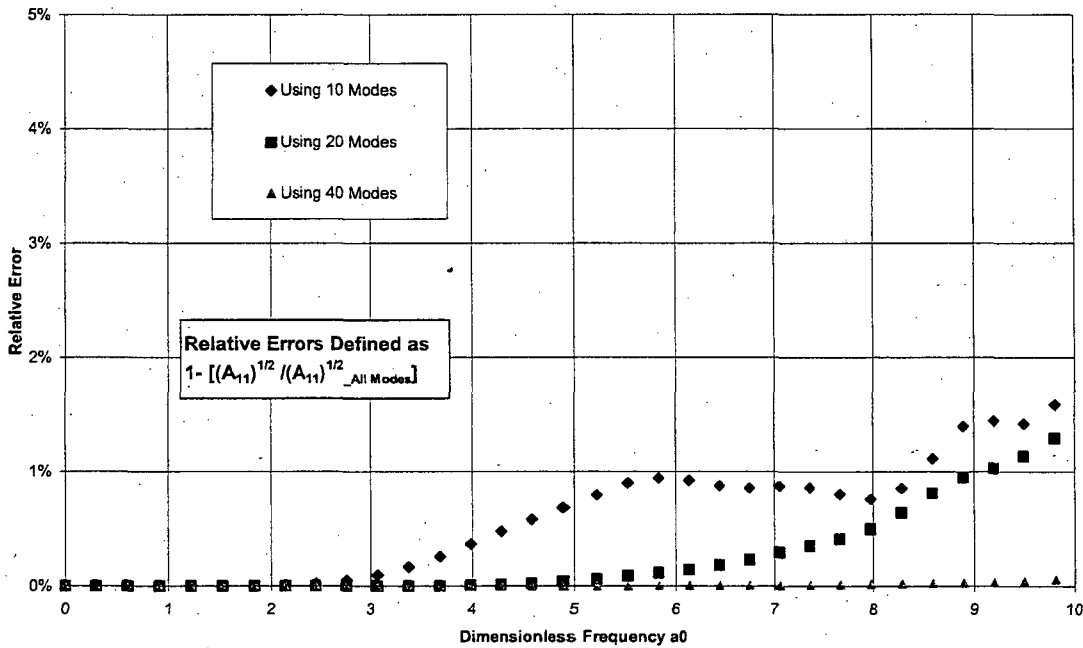


Figure 6.3

Vertical Transfer Functions at Center of a Massless Circular Foundation
Incoherent Runs

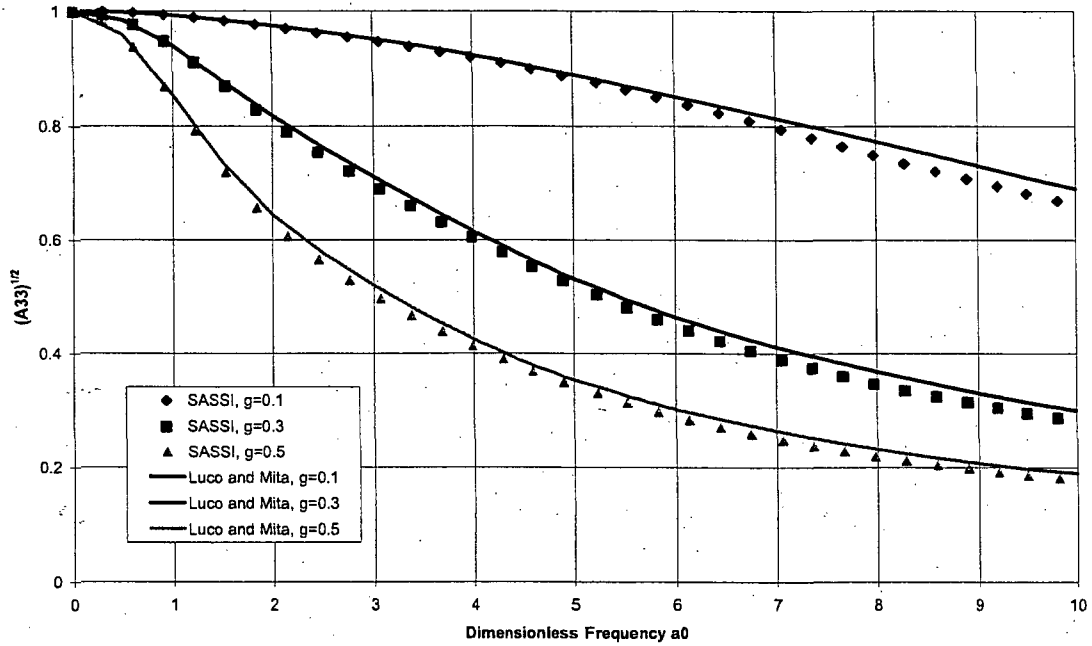


Figure 6.4

Truncation Errors Using Limited Spatial Modal Solutions
Vertical Transfer Functions. At Center of Rigid Massless Disk, $\gamma = 0.5$

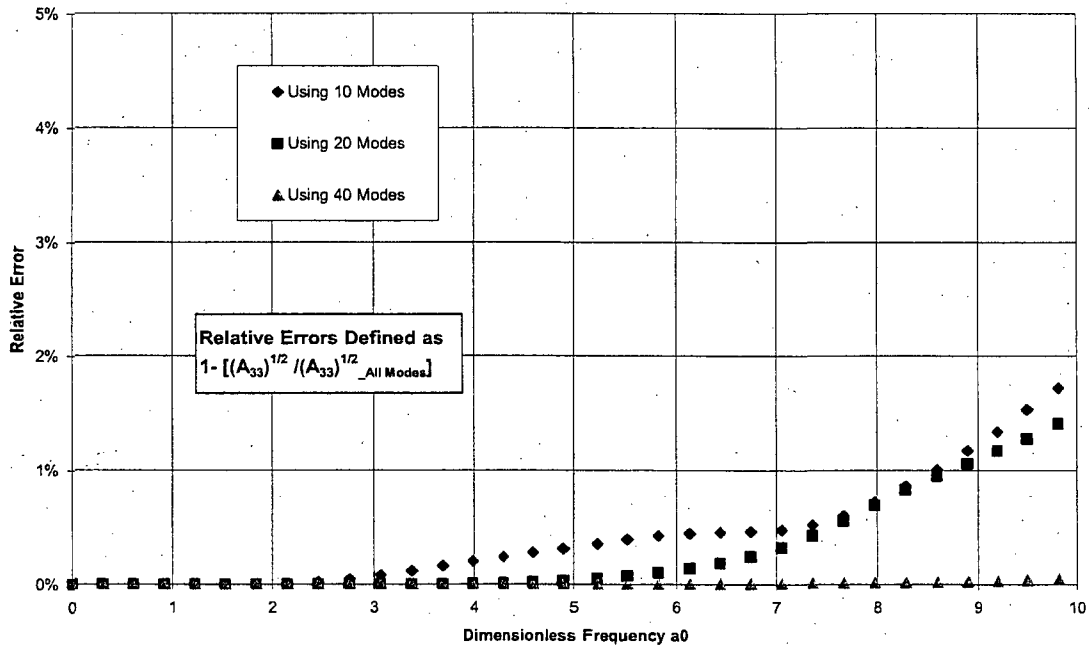


Figure 6.5

Rocking Transfer Functions at Center of a Massless Circular Foundation
Incoherent Runs

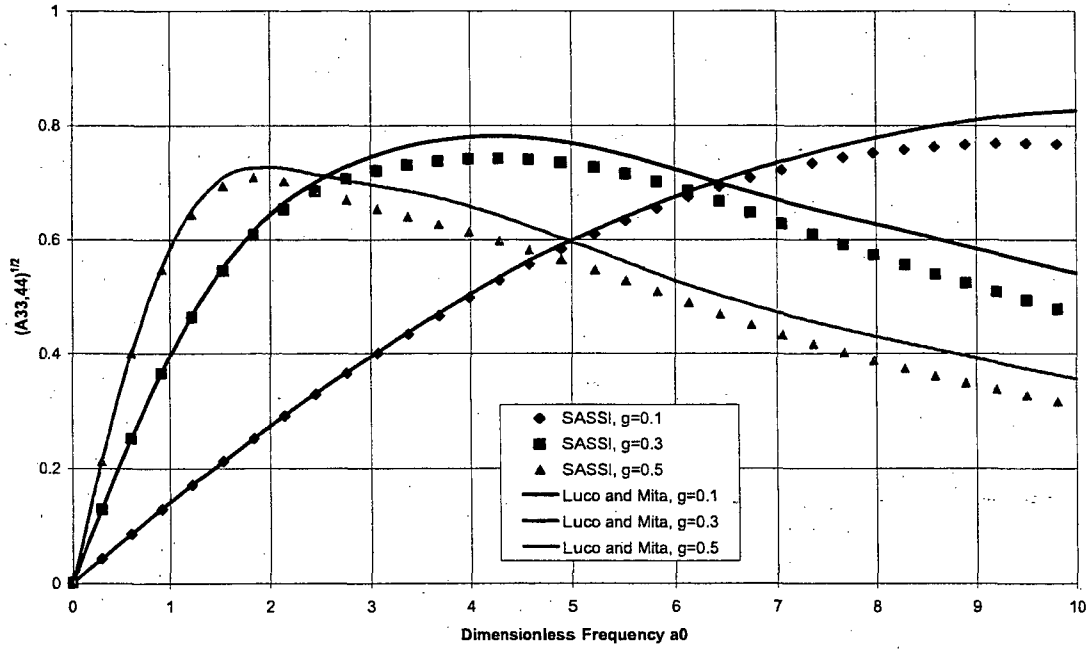


Figure 6.6

Truncation Errors Using Limited Spatial Modal Solutions
Rocking Transfer Functions. At Center of Rigid Massless Disk, $\gamma = 0.5$

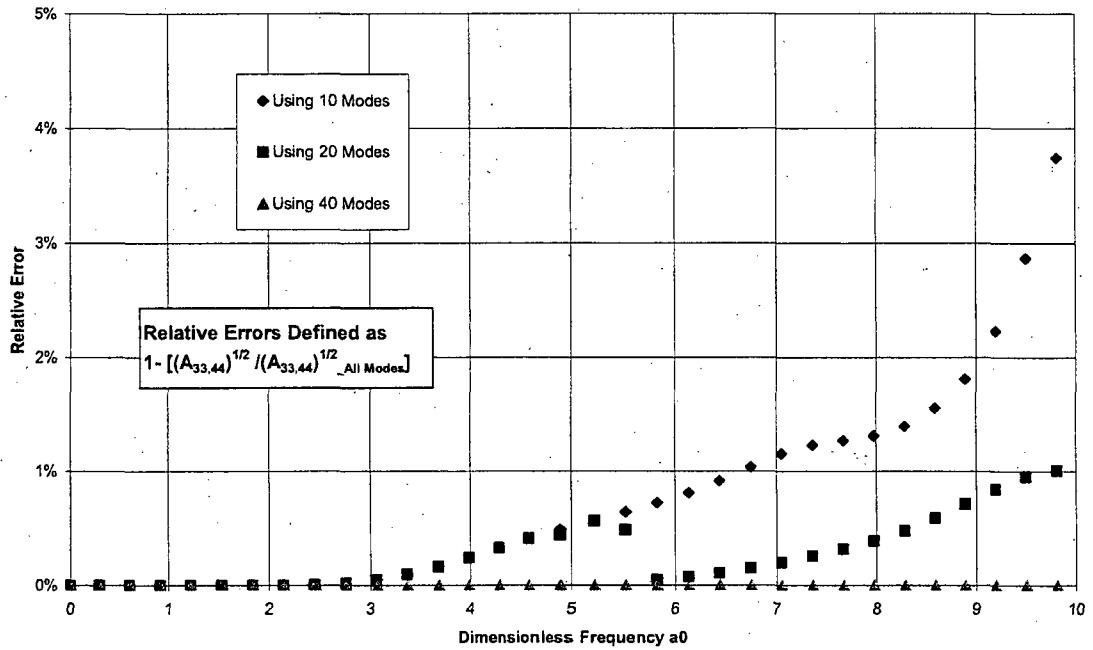


Figure 6.7
Torsional Transfer Functions at Center of a Massless Circular Foundation
Incoherent Runs

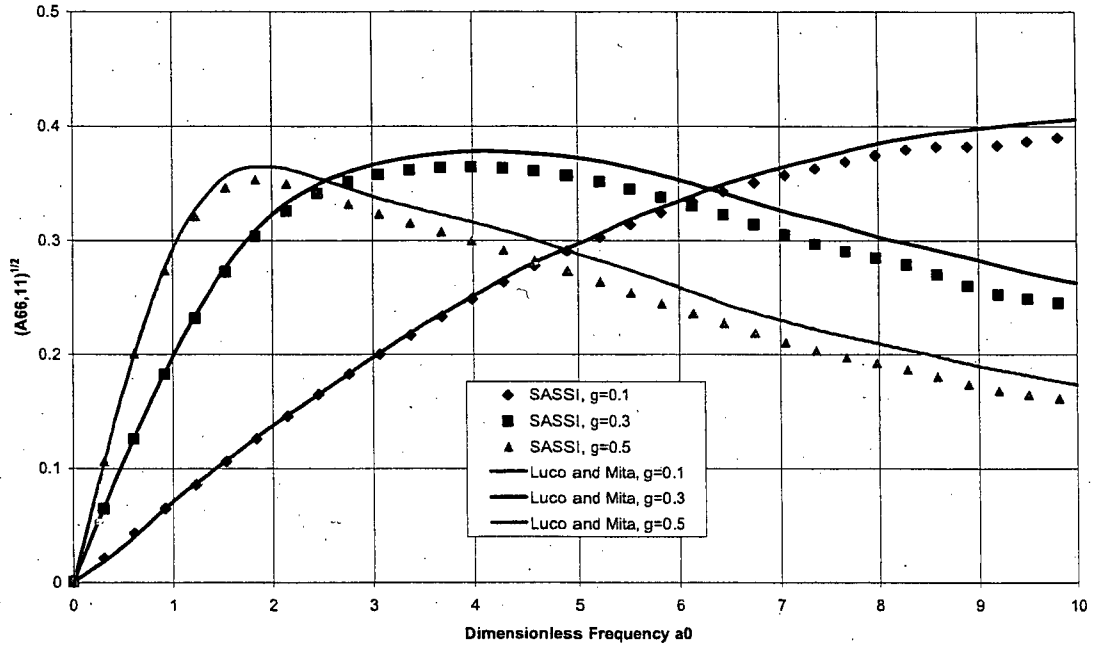
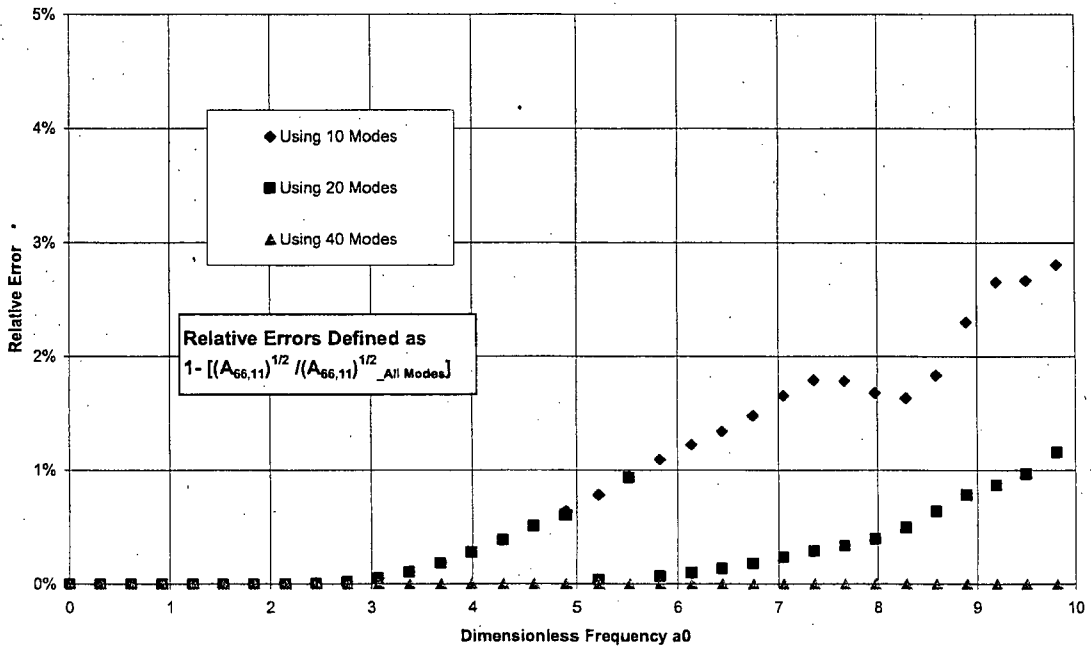


Figure 6.8
Truncation Errors Using Limited Spatial Modal Solutions
Torsional Transfer Functions. At Center of Rigid Massless Disk, $\gamma = 0.5$



Example 2

Mita and Luco (1986) published analytical results for the responses of a cylindrical building on a homogeneous half-space subjected to incoherent ground motions. The coherency function defined in Equation (2.1) is used in this paper. A sketch of the cylindrical building is shown in Figure 6.9.

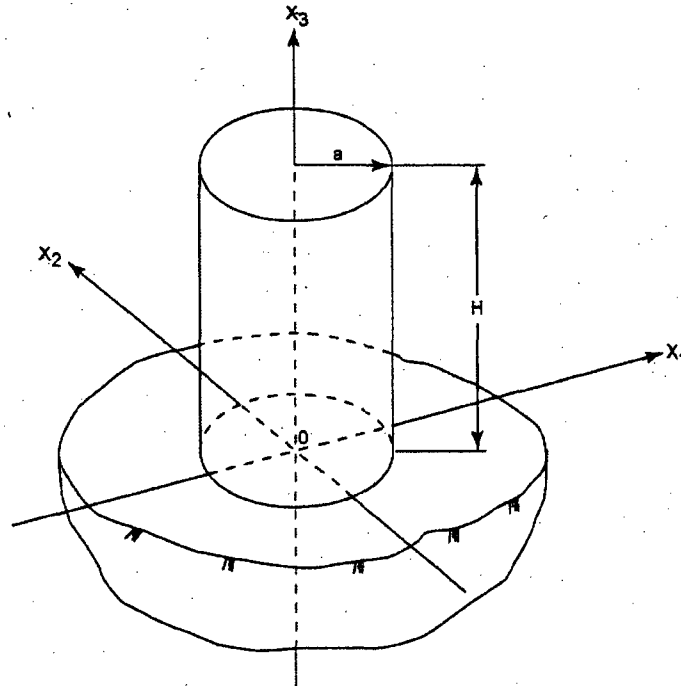


Figure 6.9 A sketch of the Building Model

The Building has the following properties:

Radius	10 m
Height	40 m
Total Mass:	10^7 kg

Fixed Base Natural Frequencies:

Horizontal	2, 6, 10, 14, 18 Hz
Vertical:	3, 9, 15, 21, 27 Hz

Structural Damping	0.02
--------------------	------

And the properties of the homogeneous halfspace are:

Shear Wave Velocity	400 (m/sec)
Poisson's Ratio	0.333
Material Damping	0.02
Mass Density	1875 (kg/m ³)

This structure is analyzed by SASSI2000 following the above outlined approach. The cases of parameter $\gamma = 0$ (the coherent motion), 0.1, 0.3 and 0.5 are analyzed. Results of SASSI2000 analyses are compared with Mita and Luco's analytical results, as shown at selected locations in Figures 6.10, 6.12, 6.14, 6.16, 6.18, 6.20 and 6.22. SASSI numerical model for this problem has a total of 69 interaction nodes, thus a total of 69 spatial modes may be utilized in calculating the incoherent responses. All results shown above are computed using all 69 modes. As shown in the figures, agreement between these two sets of results is excellent.

A sensitivity analysis is performed on the effects of using a limited number of spatial modes. This sensitivity study is performed for the $\gamma = 0.5$ case only. Figures 6.11, 6.13, 6.15, 6.17, 6.19, 6.21 and 6.23 show the comparison plots for the responses using either 69 modes or 10 modes, and the relative errors induced in using 10 modes only.

As shown in the figures, the transfer functions generated by using 10 modal solutions or by using 69 modal solutions are indistinguishable for the entire frequency range, and the maximum relative errors induced in using 10 modes only never exceeds 1% for all solutions at all locations, even at the highest frequency considered. Thus it can be concluded that for the SSI analysis of this building model, 10 spatial modes are sufficient in capture the effect of incoherent ground motions.

Figure 6.10

Horizontal Motions due to Horizontal Shaking. At Base-Center $|\Delta_1 / U_{gH}|$

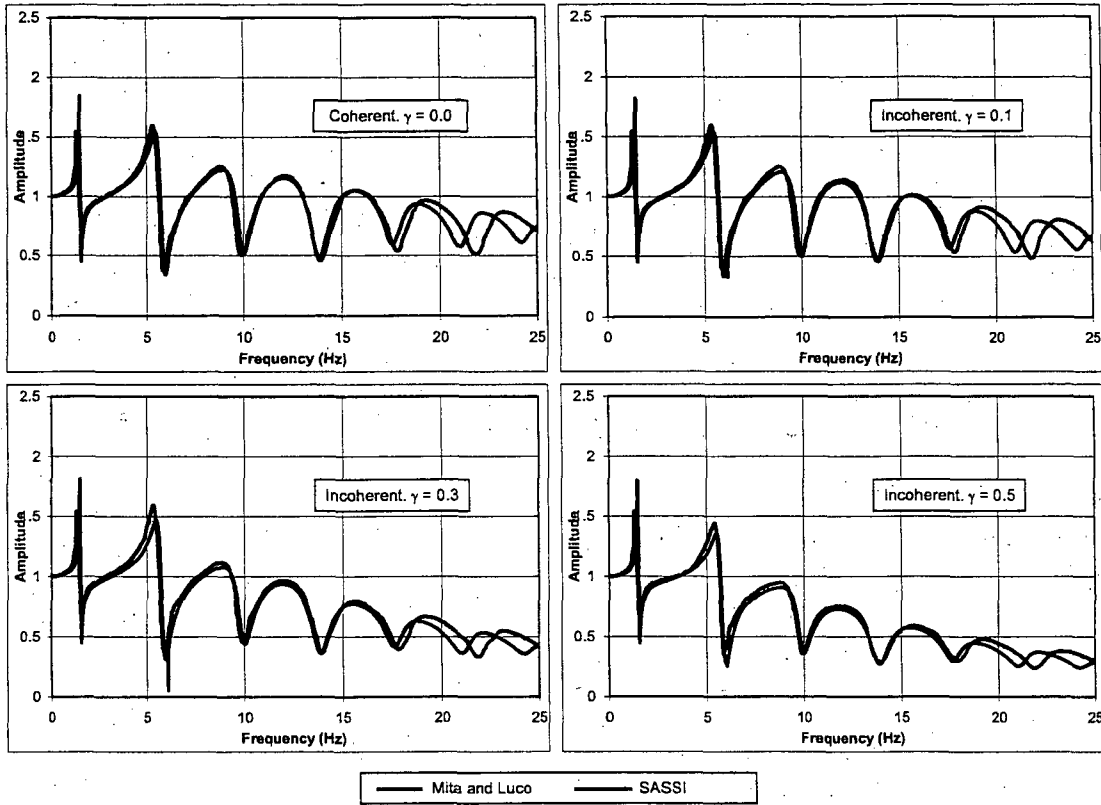


Figure 6.11

Effects of Using Limited Spatial Modal Solutions. Mita-Luoco Cylindrical Building
Horizontal Motions due to Horizontal Shaking. At Base-Center $|\Delta_1 / U_{gH}|$, $\gamma = 0.5$

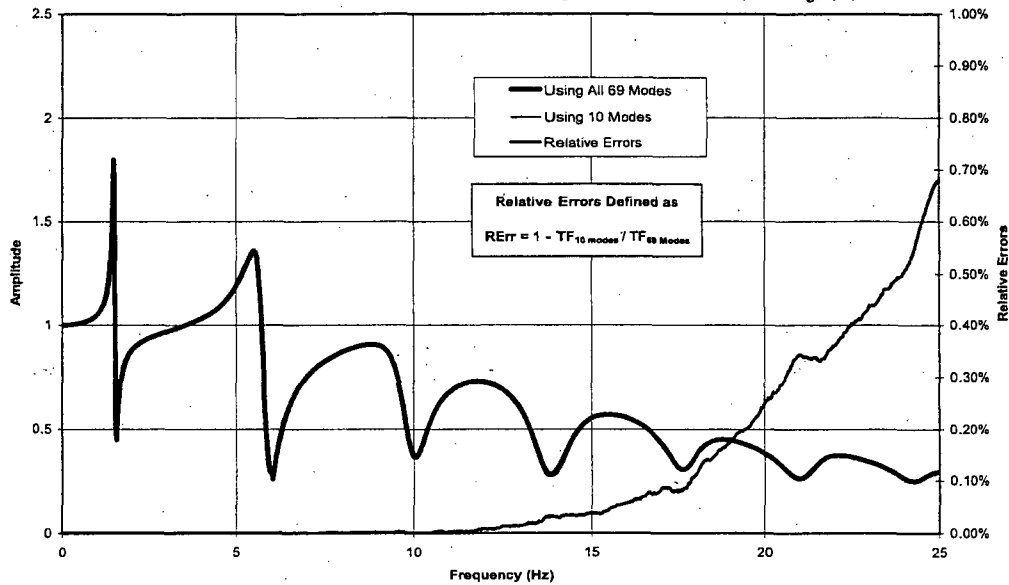


Figure 6.12

Vertical Motions due to Vertical Shaking. At Base-Center $|\Delta_3 / U_{gv}|$

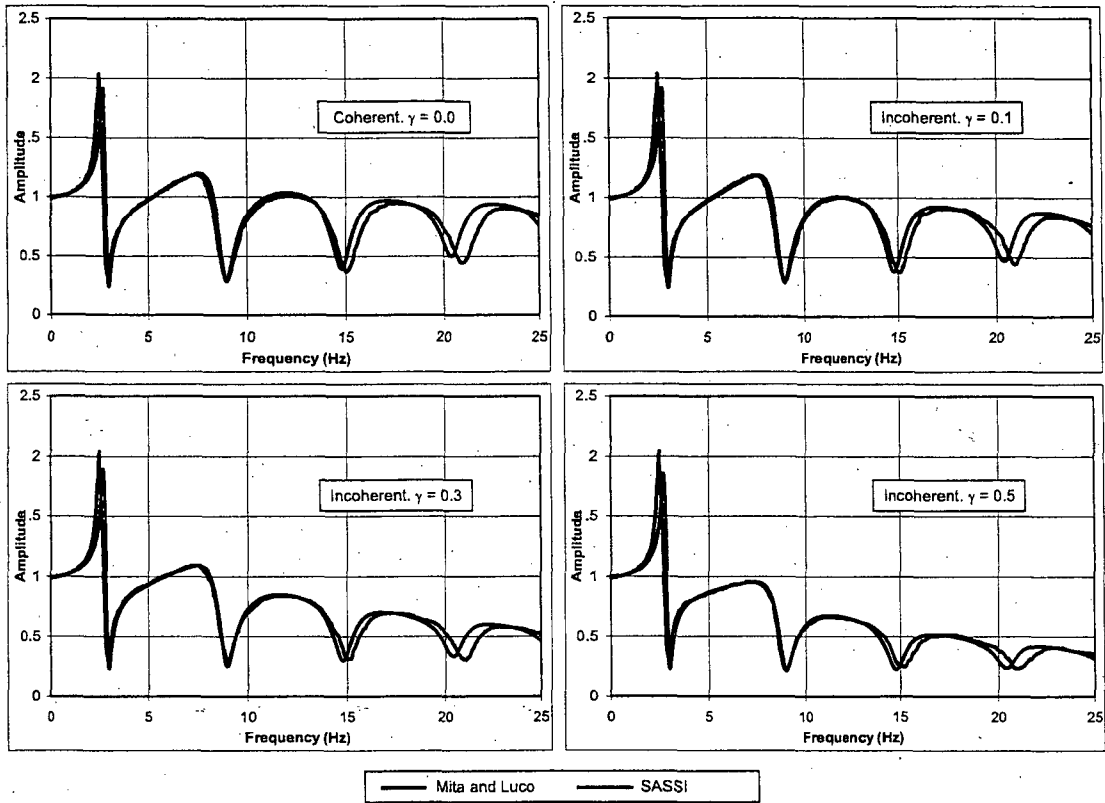


Figure 6.13

Effects of Using Limited Spatial Modal Solutions. Mita-Luoco Cylindrical Building
Vertical Motions due to Vertical Shaking. At Base-Center $|\Delta_3 / U_{gv}|$, $\gamma = 0.5$

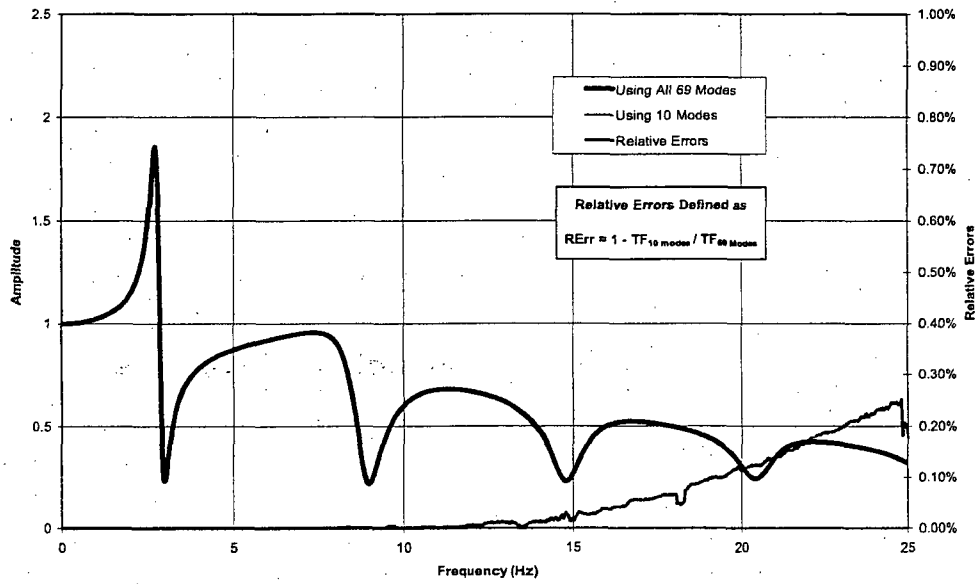


Figure 6.14

Horizontal Motions due to Vertical Shaking. At Base-Center $|\Delta_1 / U_{gV}|$

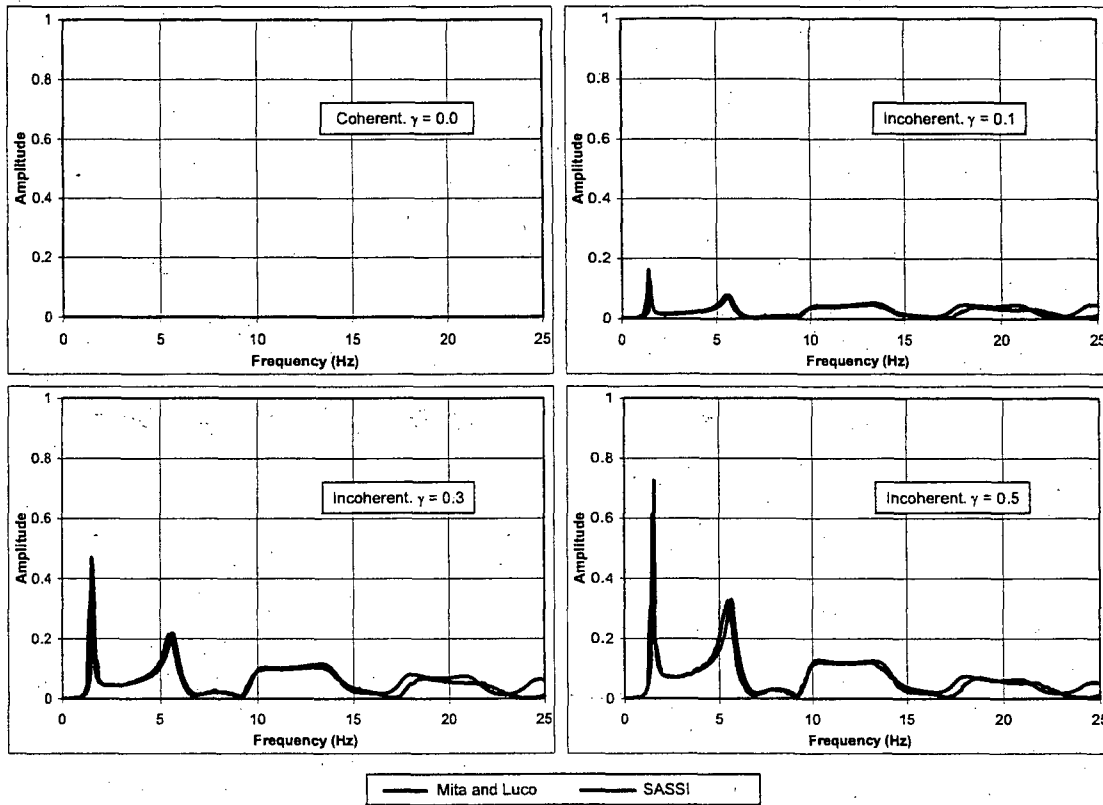


Figure 6.15

Effects of Using Limited Spatial Modal Solutions. Mita-Luco Cylindrical Building
Horizontal Motions due to Vertical Shaking. At Base-Center $|\Delta_1 / U_{gV}|$, $\gamma = 0.5$

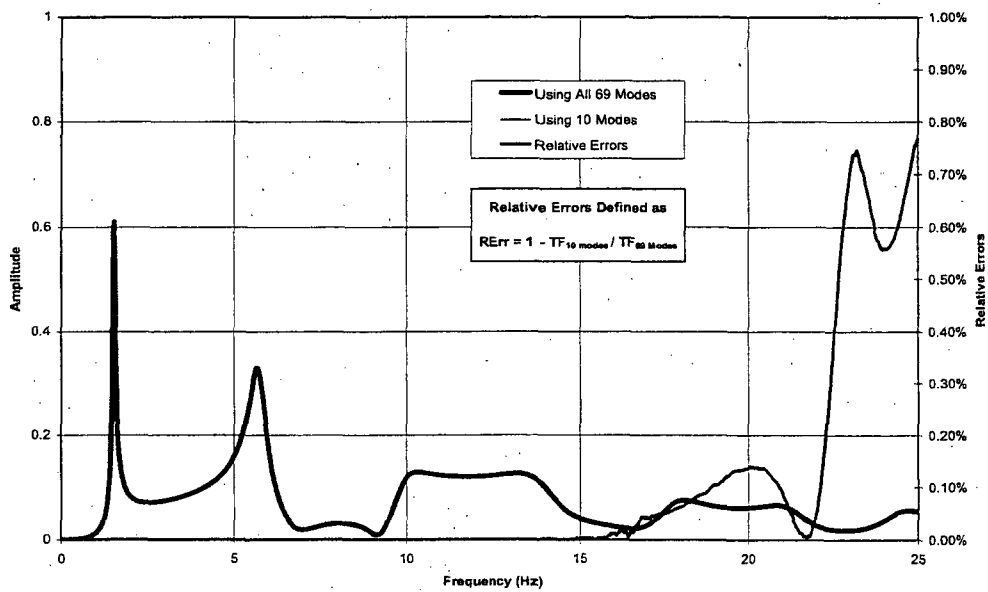


Figure 6.16

Vertical Motions due to Vertical Shaking. At Base-Edge $|\Delta_3 / U_{gV}|$

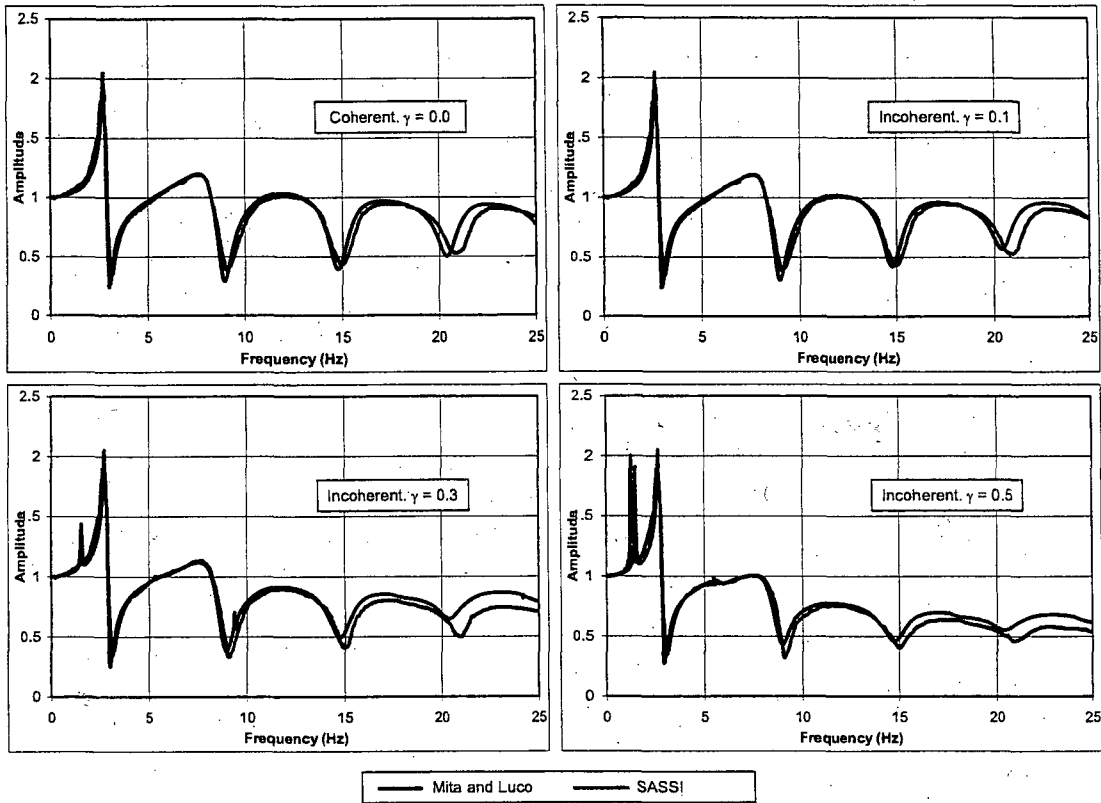


Figure 6.17

Effects of Using Limited Spatial Modal Solutions. Mita-Luco Cylindrical Building
Vertical Motions due to Vertical Shaking. At Base-Edge $|\Delta_3 / U_{gV}|, \gamma = 0.5$

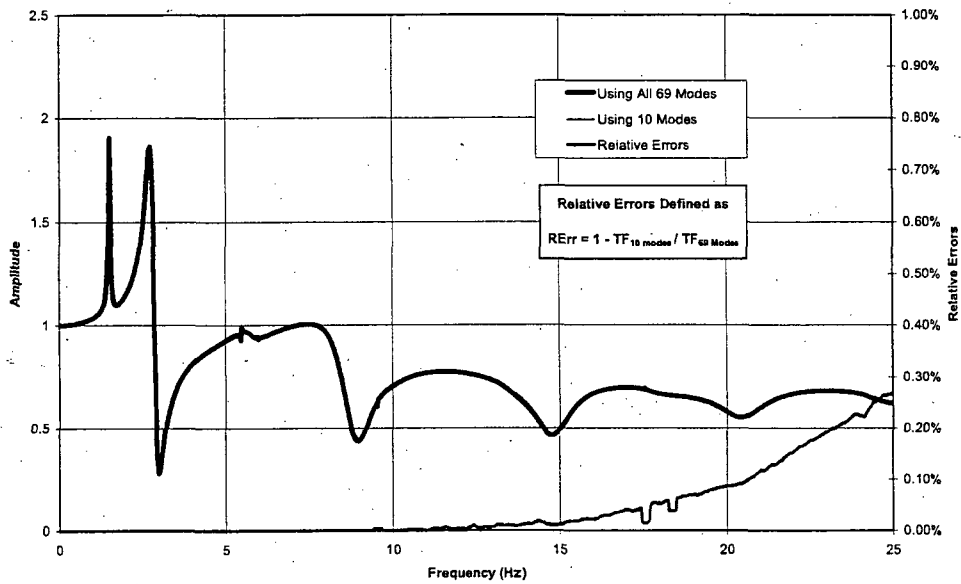


Figure 6.18

Horizontal Motions due to Horizontal Shaking. At Top-Center $|\Delta_1 / U_{gH}|$

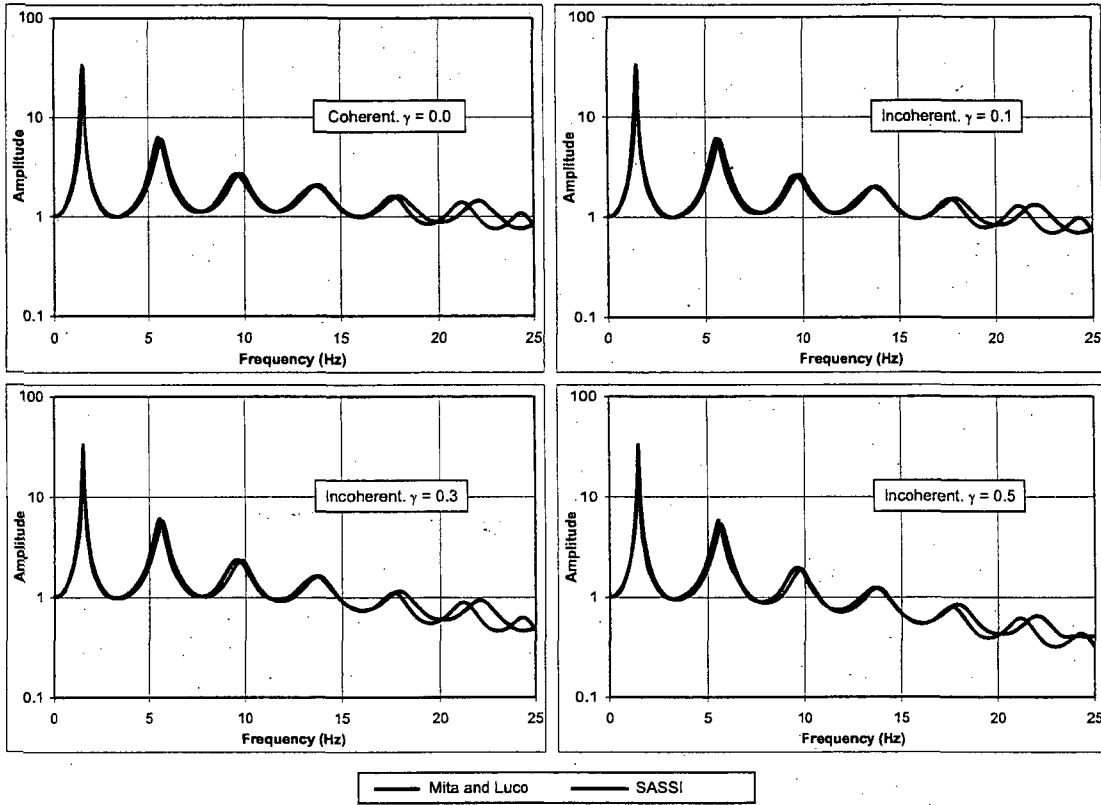


Figure 6.19

Effects of Using Limited Spatial Modal Solutions. Mita-Luco Cylindrical Building
Horizontal Motions due to Horizontal Shaking. At Top-Center $|\Delta_1 / U_{gH}| \cdot \gamma = 0.5$

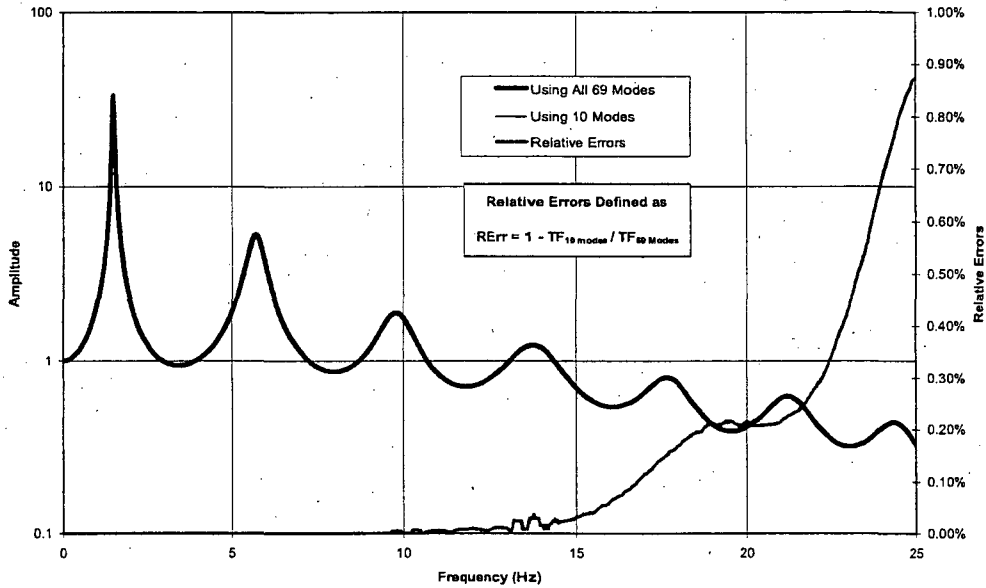


Figure 6.20

Vertical Motions due to Vertical Shaking. At Top-Center $|\Delta_3 / U_{gv}|$

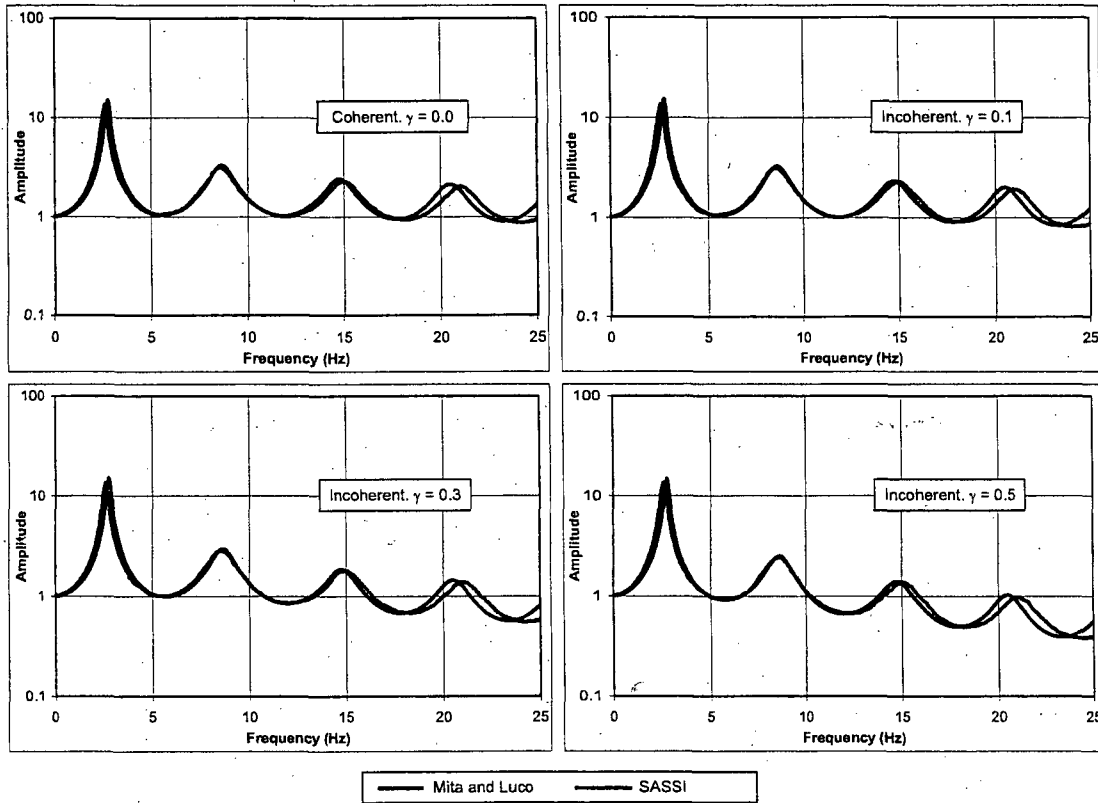


Figure 6.21

Effects of Using Limited Spatial Modal Solutions. Mita-Luoco Cylindrical Building
Vertical Motions due to Vertical Shaking. At Top-Center $|\Delta_3 / U_{gv}|$. $\gamma = 0.5$

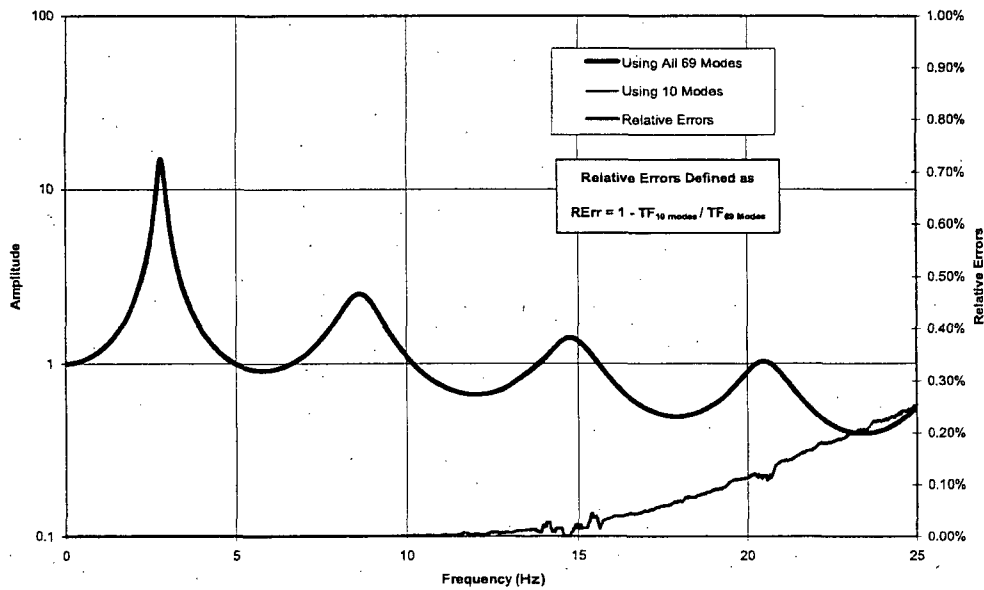


Figure 6.22

Vertical Motions due to Vertical Shaking. At Top-Edge $|\Delta_3 / U_{gV}|$

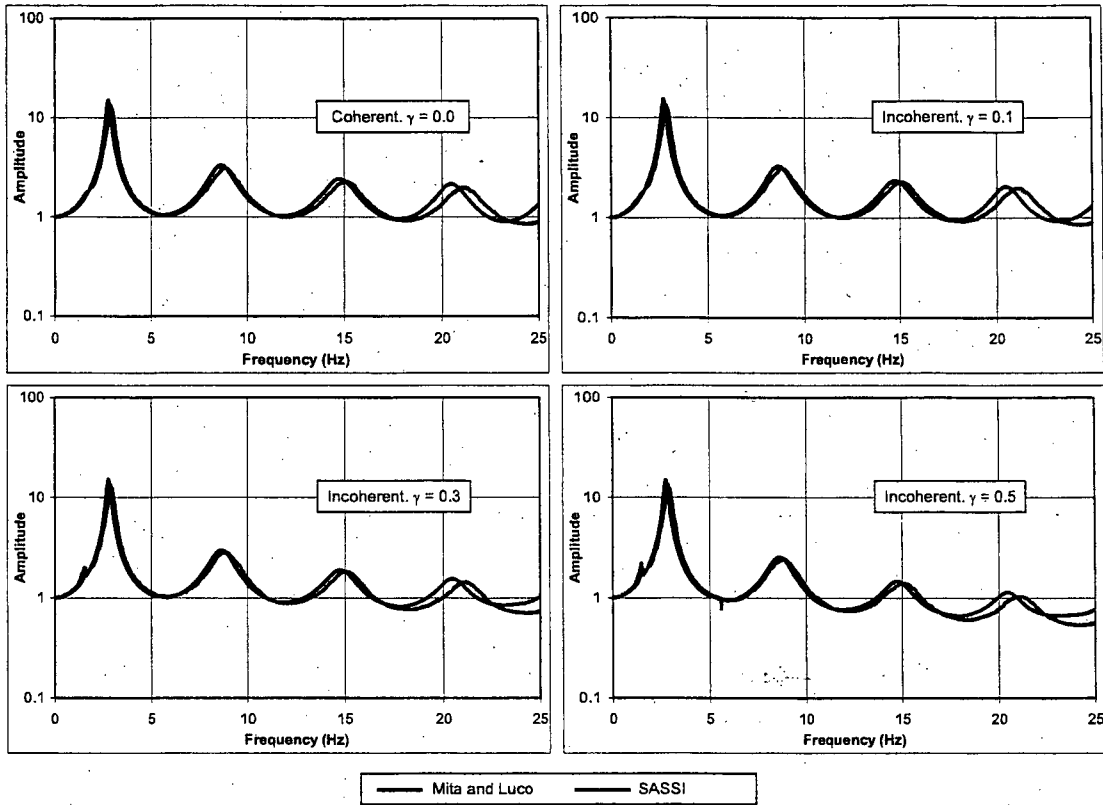
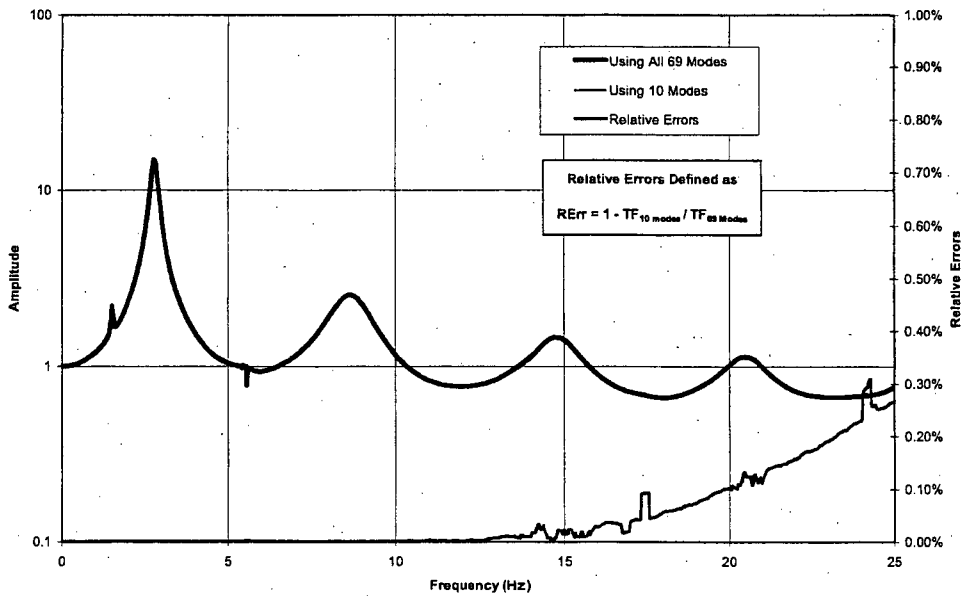


Figure 6.23

Effects of Using Limited Spatial Modal Solutions. Mita-Luco Cylindrical Building
Vertical Motions due to Vertical Shaking. At Top-Edge $|\Delta_3 / U_{gV}|$, $\gamma = 0.5$



Additional Verification Examples

In addition to the above verification examples, a typical standard nuclear power plant model has been analyzed using the Computer Programs SASSI and CLASSI (EPRI, 2007). The details of the multi-stick model and the input motion as well as the site properties are fully described in the EPRI report. In the EPRI report, the results of analysis are compared at numerous locations in the structure for both coherent motions and incoherent motions with Abrahamson model. The SASSI2000-SRSS results are compared with the results of number of other methods. In particular, solutions from the CLASSI-SRSS method and the SASSI-Simulation method are found to be in close agreement with the SASSI-SRSS method. All SASSI-SRSS results presented in the EPRI report are computed using 10 spatial modal solutions. These results are not repeated in here to avoid duplication.

A sensitivity analysis is performed on the effects of using a limited number of spatial modes only. SASSI numerical model for this standard nuclear plant has a total of 169 interaction nodes, thus a total of 169 spatial modes may be utilized in calculating the incoherent responses. For the purpose of this sensitivity analysis, the solutions for all 169 spatial modes are generated and transfer functions (TF) utilizing all modal solutions are computed.

Figures 6.24 through 6.44 show comparison plots of the TFs generated using 10 modes and 169 modes. The TFs are for X-X, Y-Y, Z-Z, X-Y, X-Z, Z-X, Z-Y directions at the three outriggers (ASB outrigger, Node 118, SCV outrigger, Node 145; and CIS outrigger, Node 229). The X-Y TF denotes X-response due to Y-shaking.

As shown in the figures, the TFs in all major directions generated by using 10 modal solutions or by using 169 modal solutions are indistinguishable for all practical purposes. It is therefore concluded that for practical applications of SASSI SSI incoherent analysis, utilization of up to 10 spatial modes shall be adequate to obtain accurate solutions.

(It should be noted that these figures are only samples at selected critical locations. Comparison plots are generated at many other locations but not presented herein due to space limitations. Observation from all comparison plots reaches the same conclusion.)

Figure 6.24

**Effects of Using Limited Spatial Modal Solutions for Incoherent Motion Analysis
X-X Transfer Functions at Node 118 (ASB Outrigger), AP1000 Outrigger Model.**

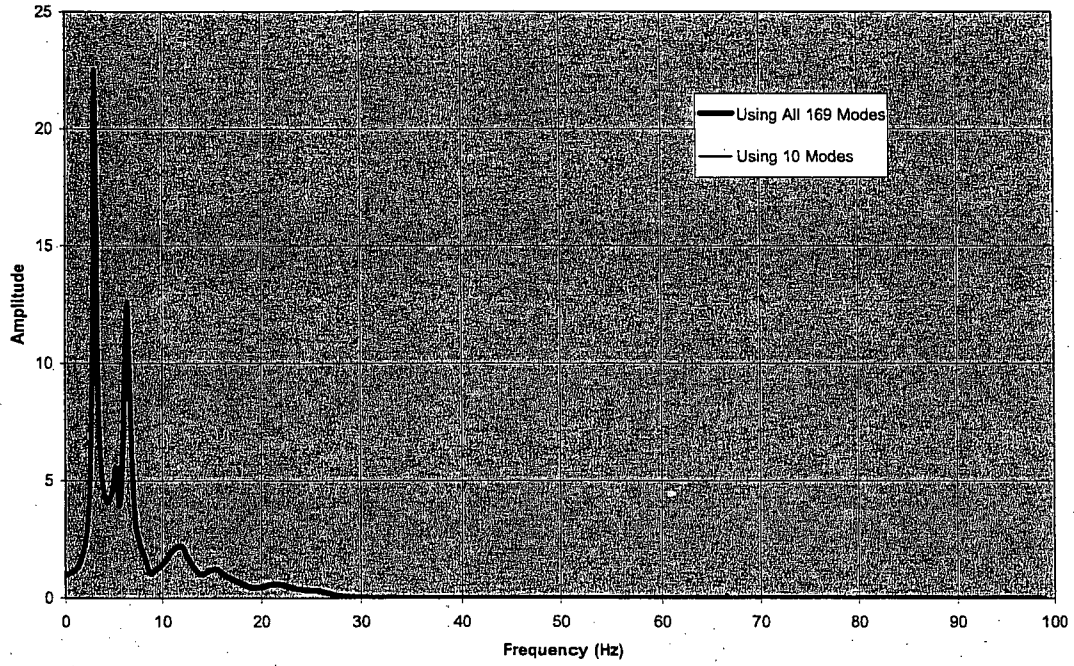


Figure 6.25

**Effects of Using Limited Spatial Modal Solutions for Incoherent Motion Analysis
Y-Y Transfer Functions at Node 118 (ASB Outrigger), AP1000 Outrigger Model.**

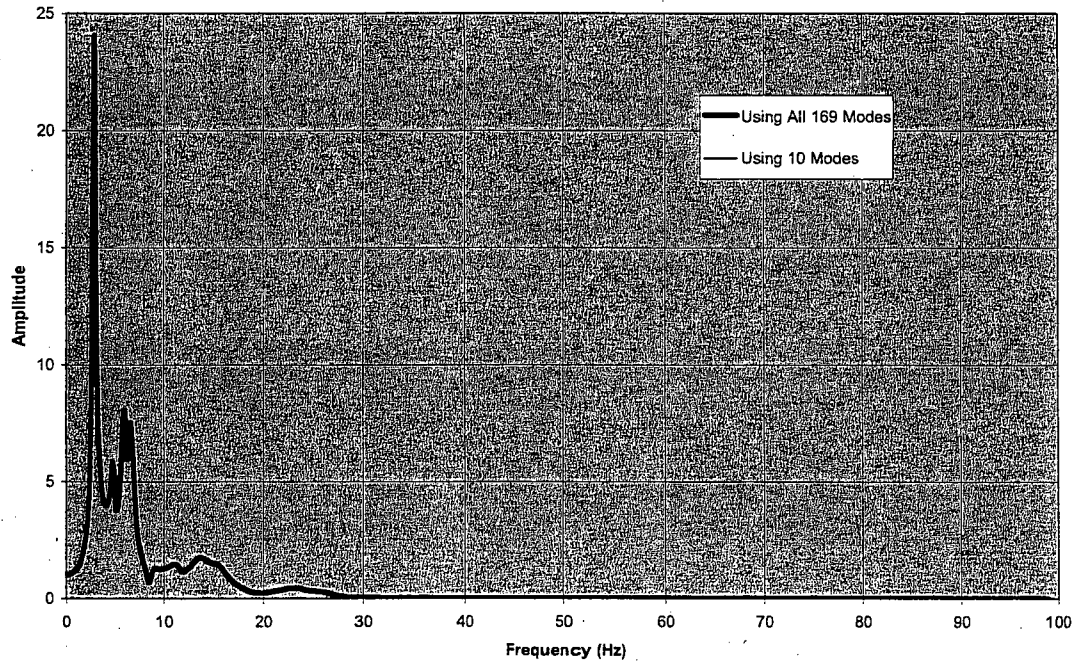


Figure 6.26

**Effects of Using Limited Spatial Modal Solutions for Incoherent Motion Analysis
Z-Z Transfer Functions at Node 118 (ASB Outrigger), AP1000 Outrigger Model.**

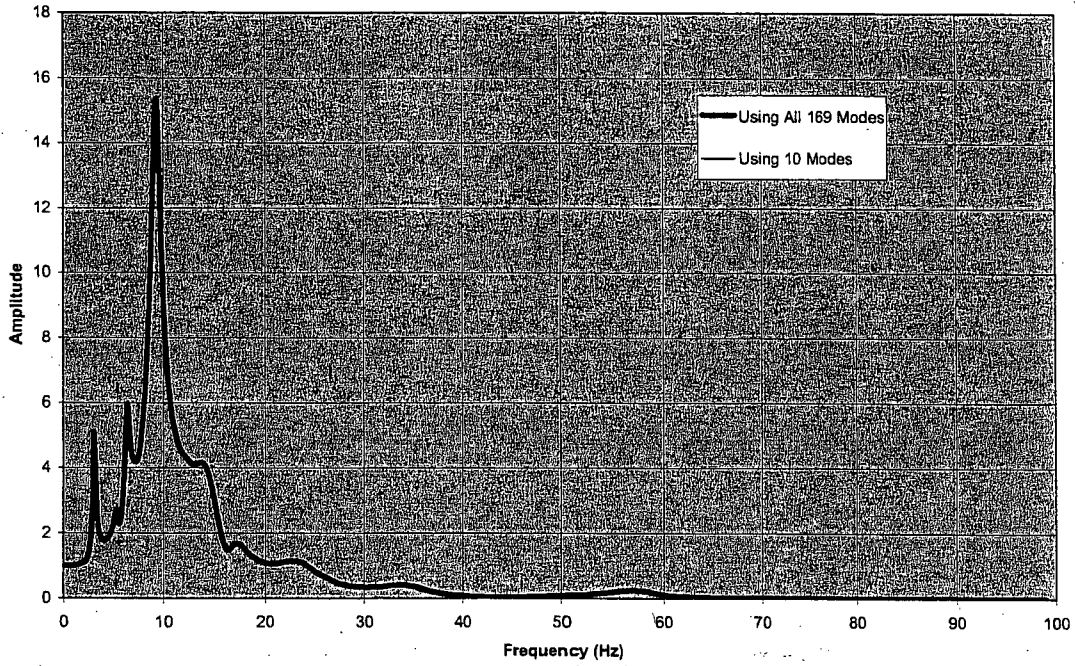


Figure 6.27

**Effects of Using Limited Spatial Modal Solutions for Incoherent Motion Analysis
X-Y Transfer Functions at Node 118 (ASB Outrigger), AP1000 Outrigger Model.**

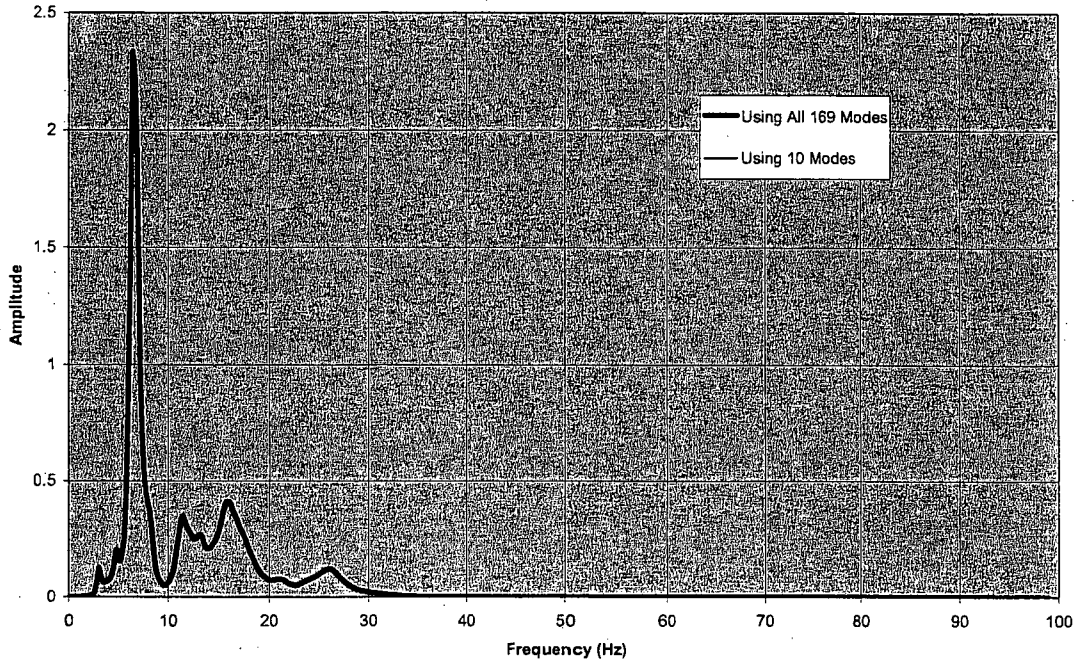


Figure 6.28

**Effects of Using Limited Spatial Modal Solutions for Incoherent Motion Analysis
X-Z Transfer Functions at Node 118 (ASB Outrigger), AP1000 Outrigger Model.**

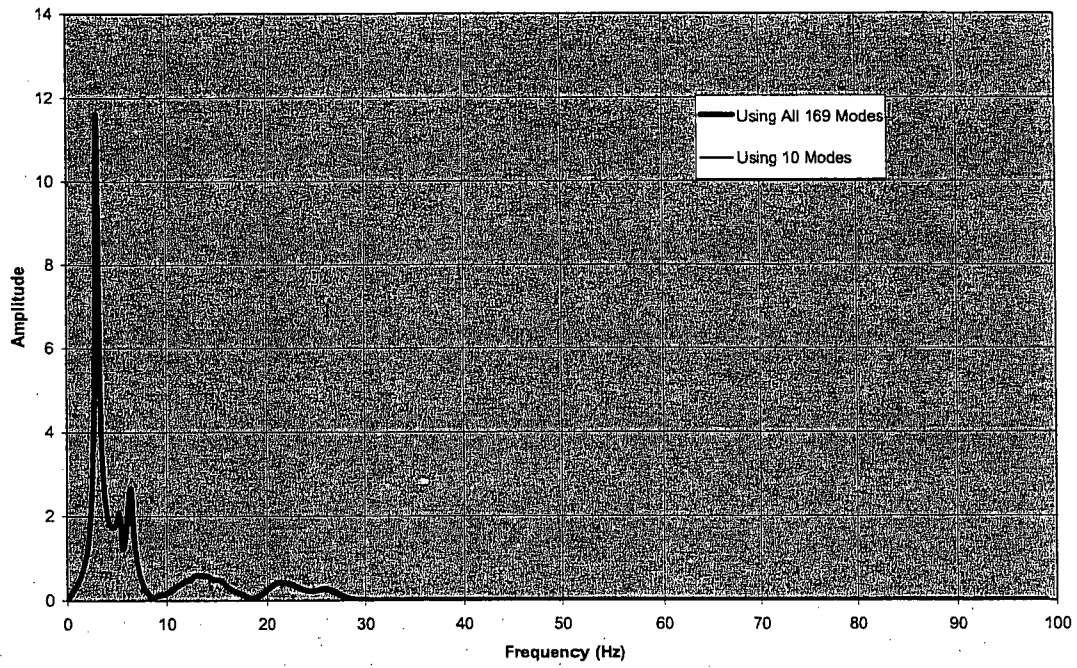


Figure 6.29

**Effects of Using Limited Spatial Modal Solutions for Incoherent Motion Analysis
Z-X Transfer Functions at Node 118 (ASB Outrigger), AP1000 Outrigger Model.**

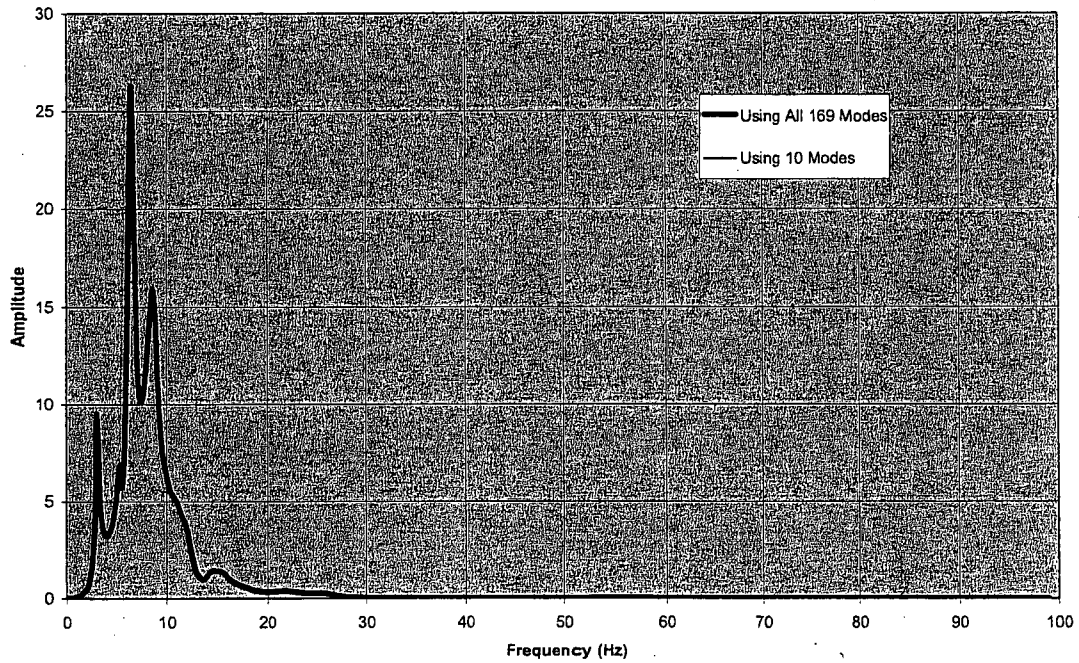


Figure 6.30

**Effects of Using Limited Spatial Modal Solutions for Incoherent Motion Analysis
Z-Y Transfer Functions at Node 118 (ASB Outrigger), AP1000 Outrigger Model.**

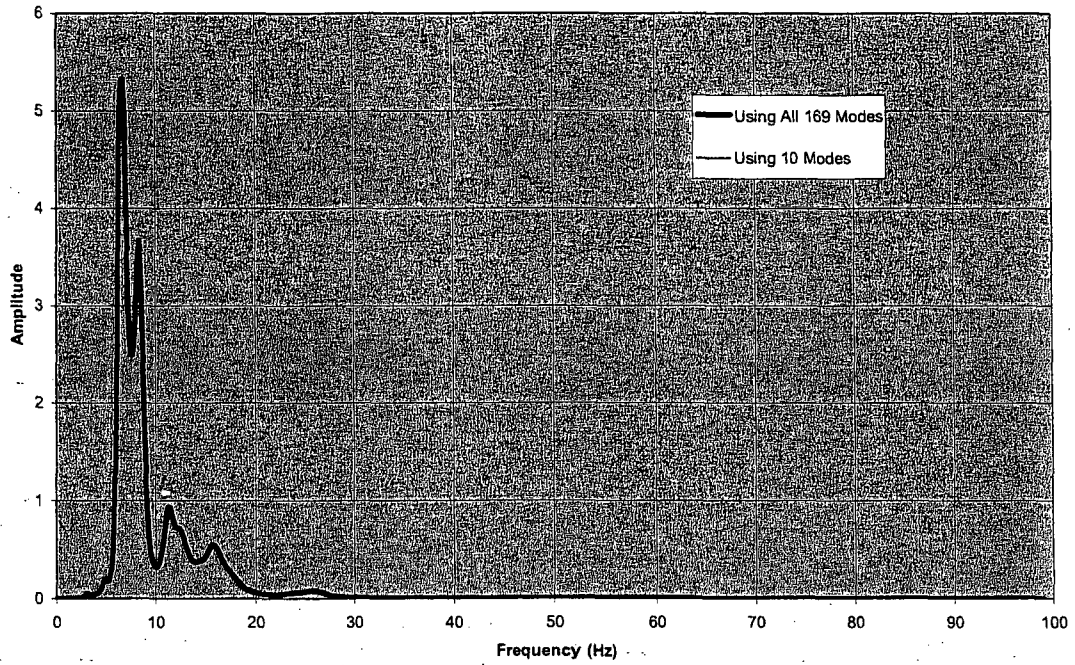


Figure 6.31

**Effects of Using Limited Spatial Modal Solutions for Incoherent Motion Analysis
X-X Transfer Functions at Node 145 (SCV Outrigger), AP1000 Outrigger Model.**

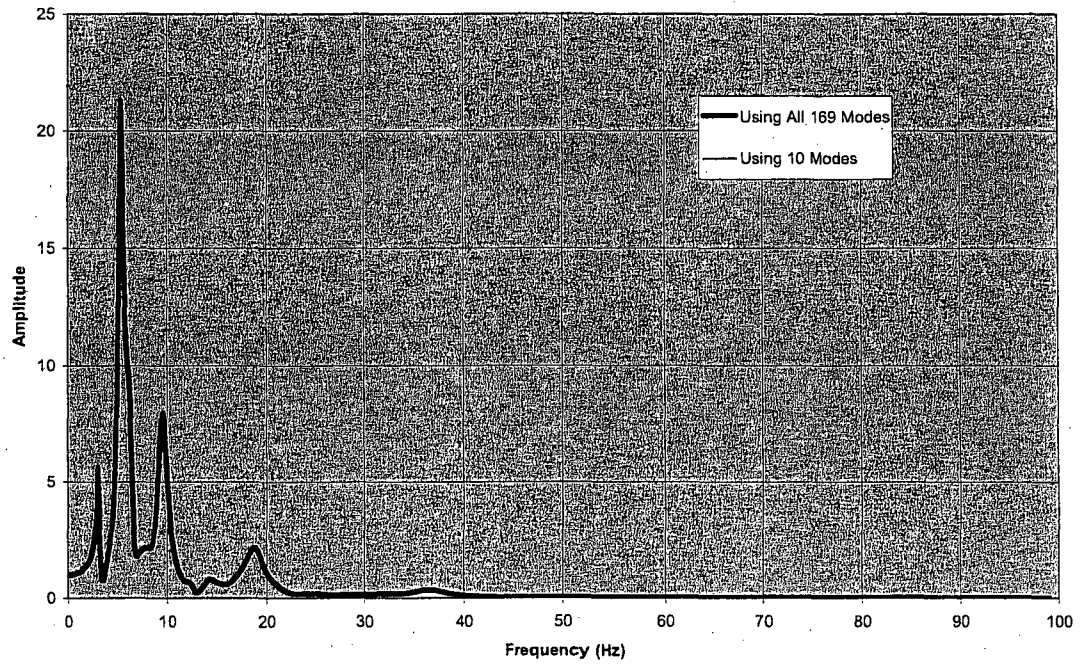


Figure 6.32

**Effects of Using Limited Spatial Modal Solutions for Incoherent Motion Analysis
Y-Y Transfer Functions at Node 145 (SCV Outrigger), AP1000 Outrigger Model.**

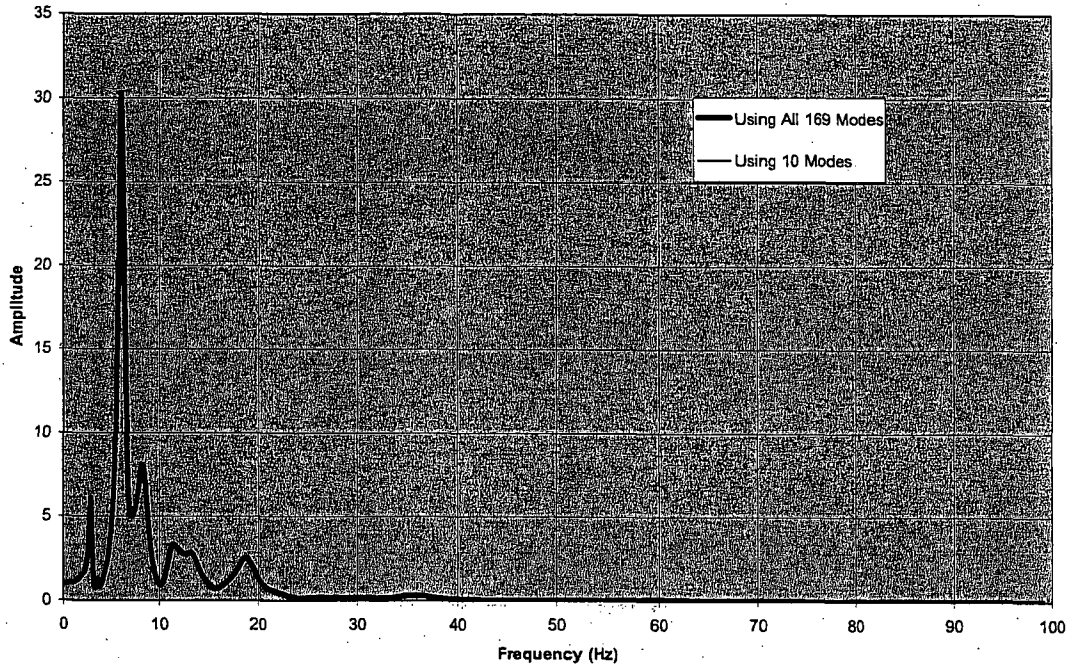


Figure 6.33

**Effects of Using Limited Spatial Modal Solutions for Incoherent Motion Analysis
Z-Z Transfer Functions at Node 145 (SCV Outrigger), AP1000 Outrigger Model.**

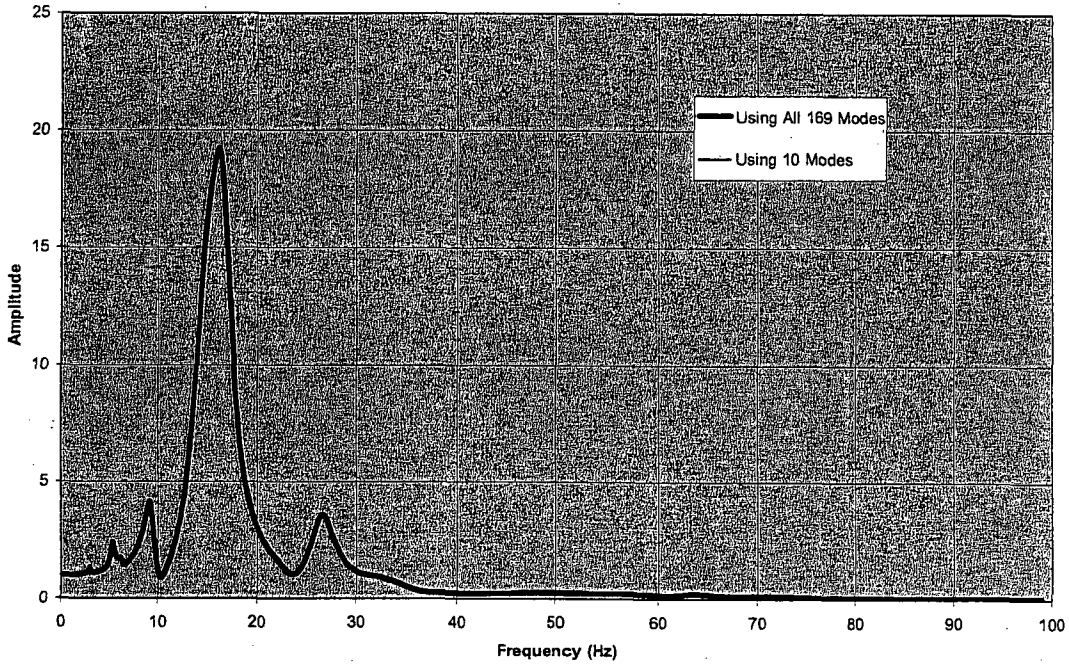


Figure 6.34

**Effects of Using Limited Spatial Modal Solutions for Incoherent Motion Analysis
X-Y Transfer Functions at Node 145 (SCV Outrigger), AP1000 Outrigger Model.**

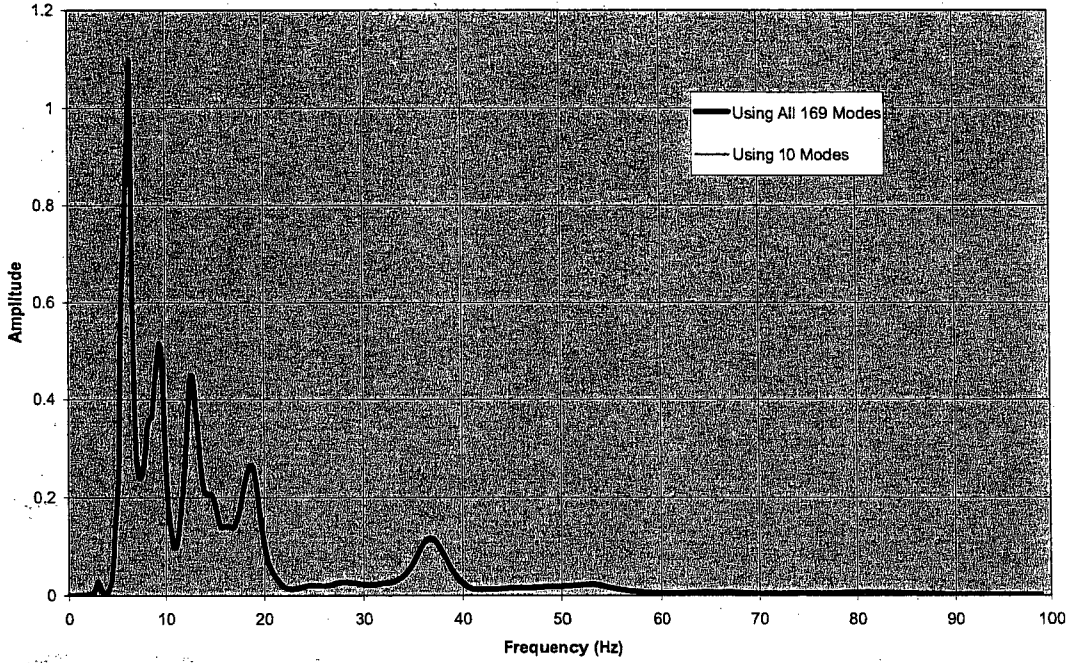


Figure 6.35

**Effects of Using Limited Spatial Modal Solutions for Incoherent Motion Analysis
X-Z Transfer Functions at Node 145 (SCV Outrigger), AP1000 Outrigger Model.**

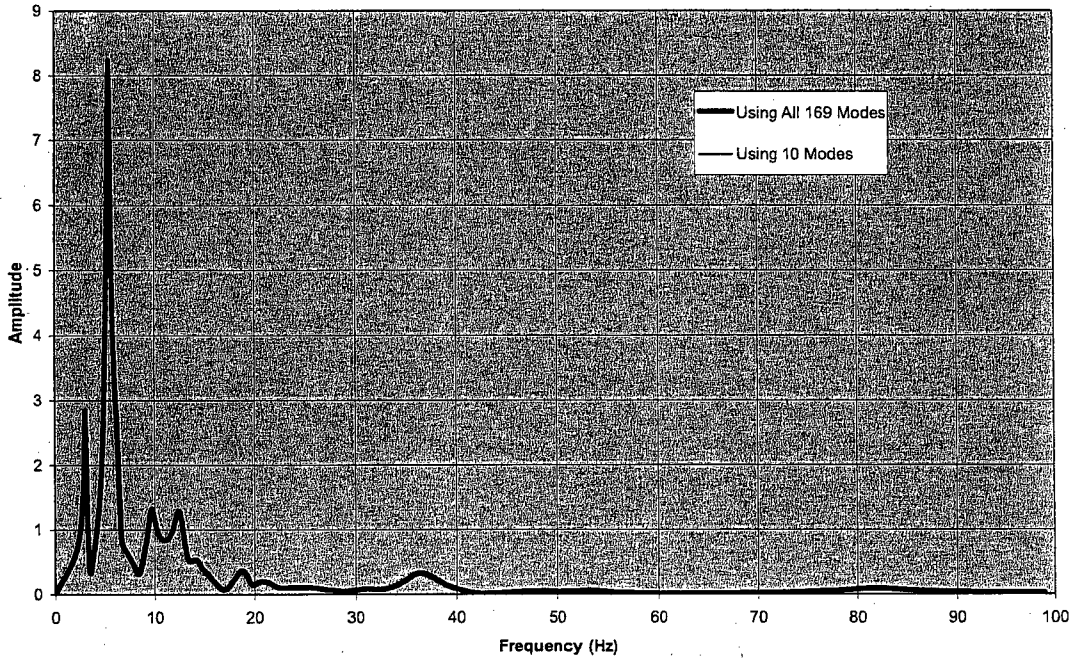


Figure 6.36

**Effects of Using Limited Spatial Modal Solutions for Incoherent Motion Analysis
Z-X Transfer Functions at Node 145 (SCV Outrigger), AP1000 Outrigger Model.**

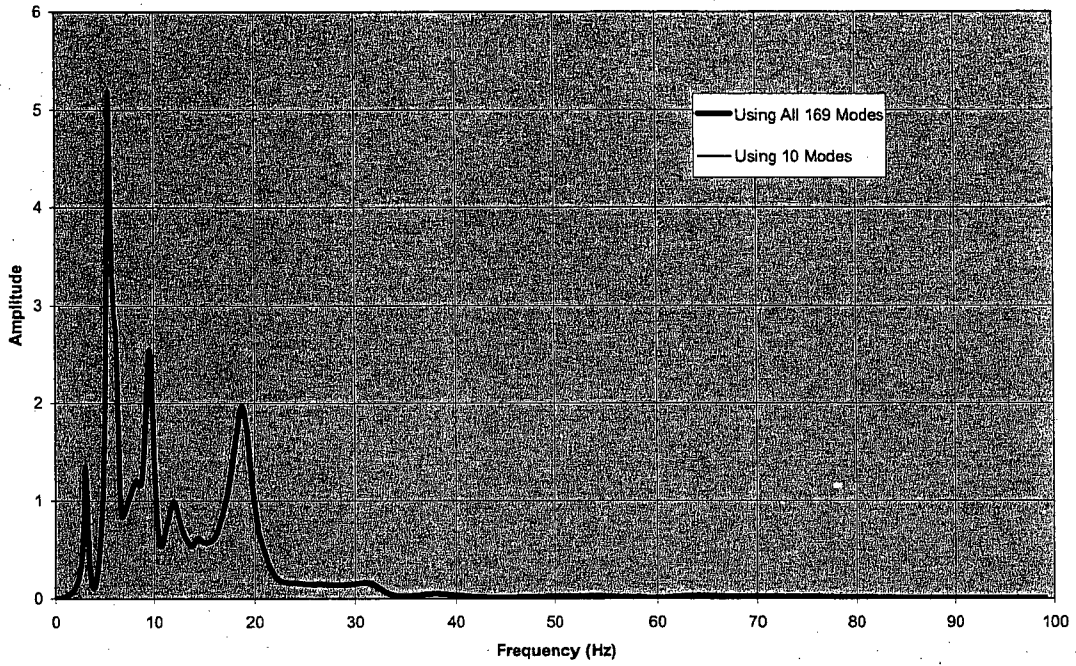


Figure 6.37

**Effects of Using Limited Spatial Modal Solutions for Incoherent Motion Analysis
Z-Y Transfer Functions at Node 145 (SCV Outrigger), AP1000 Outrigger Model.**

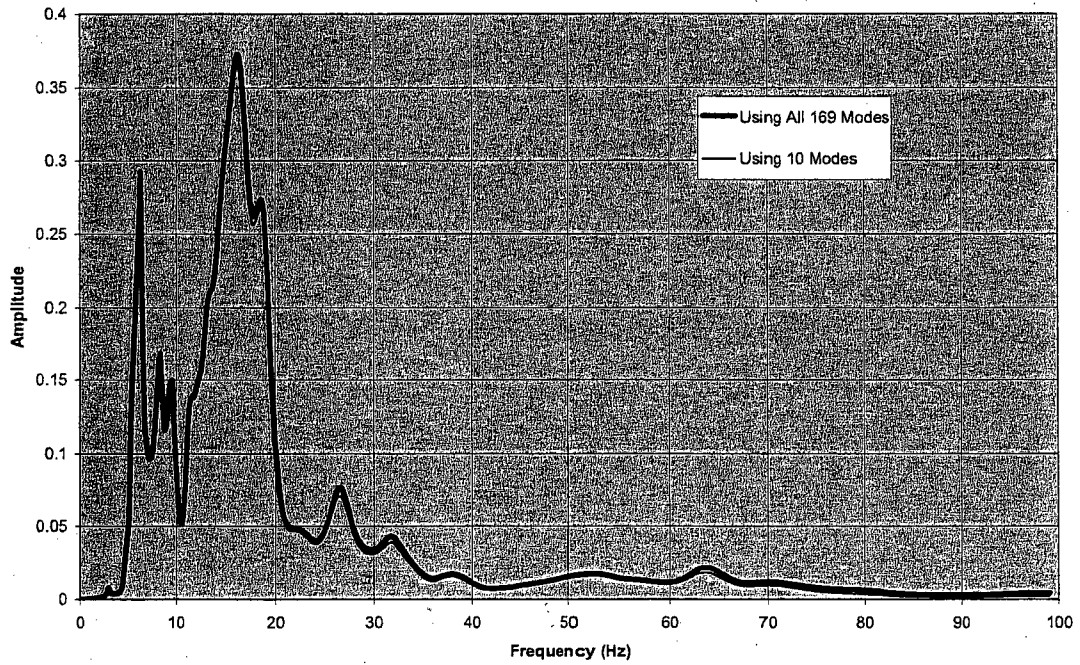


Figure 6.38

**Effects of Using Limited Spatial Modal Solutions for Incoherent Motion Analysis
X-X Transfer Functions at Node 229 (CIS Outrigger), AP1000 Outrigger Model.**

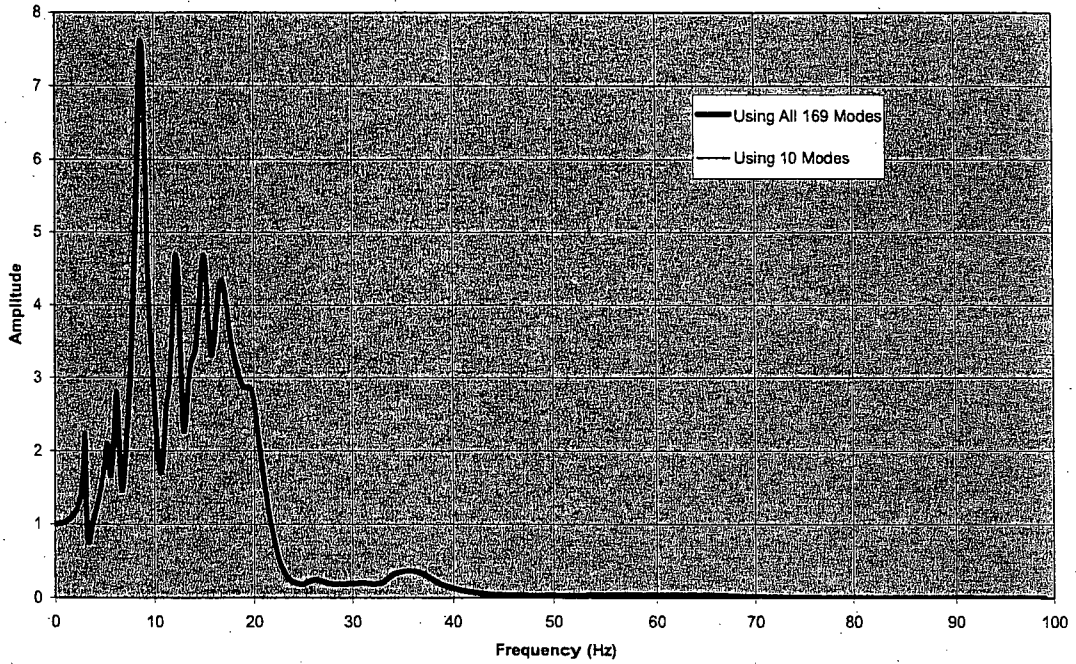


Figure 6.39

**Effects of Using Limited Spatial Modal Solutions for Incoherent Motion Analysis
Y-Y Transfer Functions at Node 229 (CIS Outrigger), AP1000 Outrigger Model.**

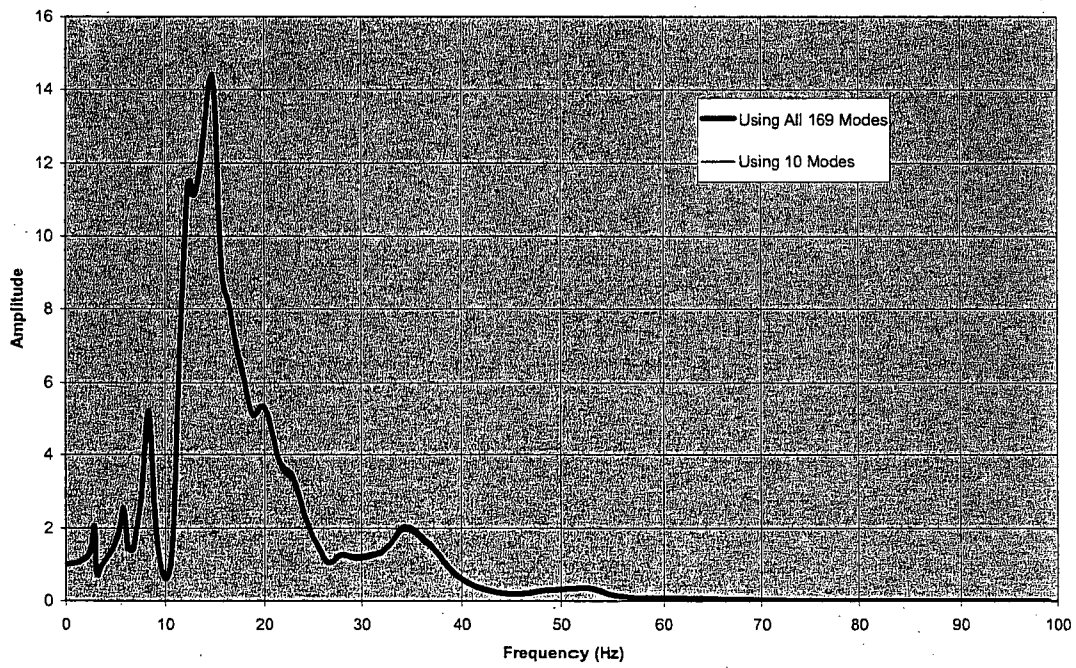


Figure 6.40

**Effects of Using Limited Spatial Modal Solutions for Incoherent Motion Analysis
Z-Z Transfer Functions at Node 229 (CIS Outrigger), AP1000 Outrigger Model.**

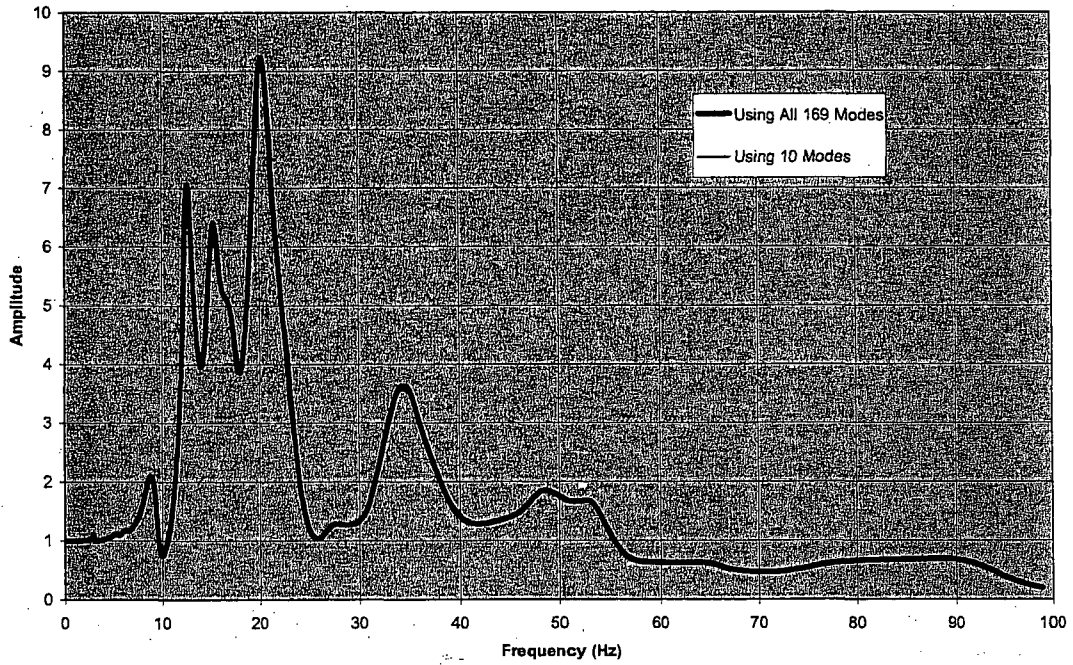


Figure 6.41

**Effects of Using Limited Spatial Modal Solutions for Incoherent Motion Analysis
X-Y Transfer Functions at Node 229 (CIS Outrigger), AP1000 Outrigger Model.**

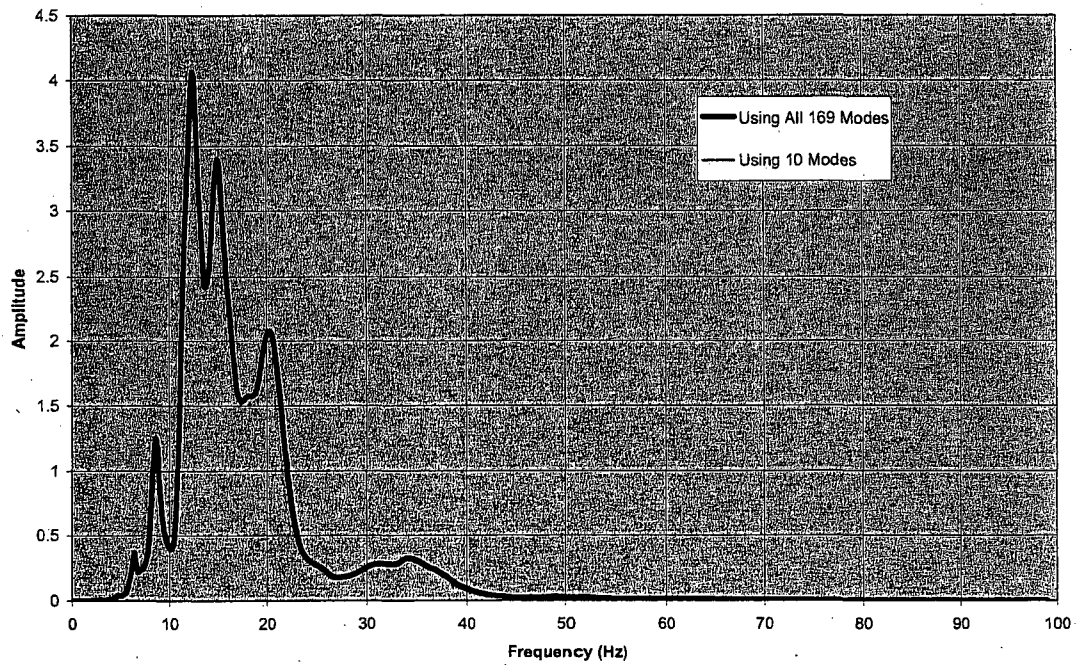


Figure 6.42

**Effects of Using Limited Spatial Modal Solutions for Incoherent Motion Analysis
X-Z Transfer Functions at Node 229 (CIS Outrigger), AP1000 Outrigger Model.**

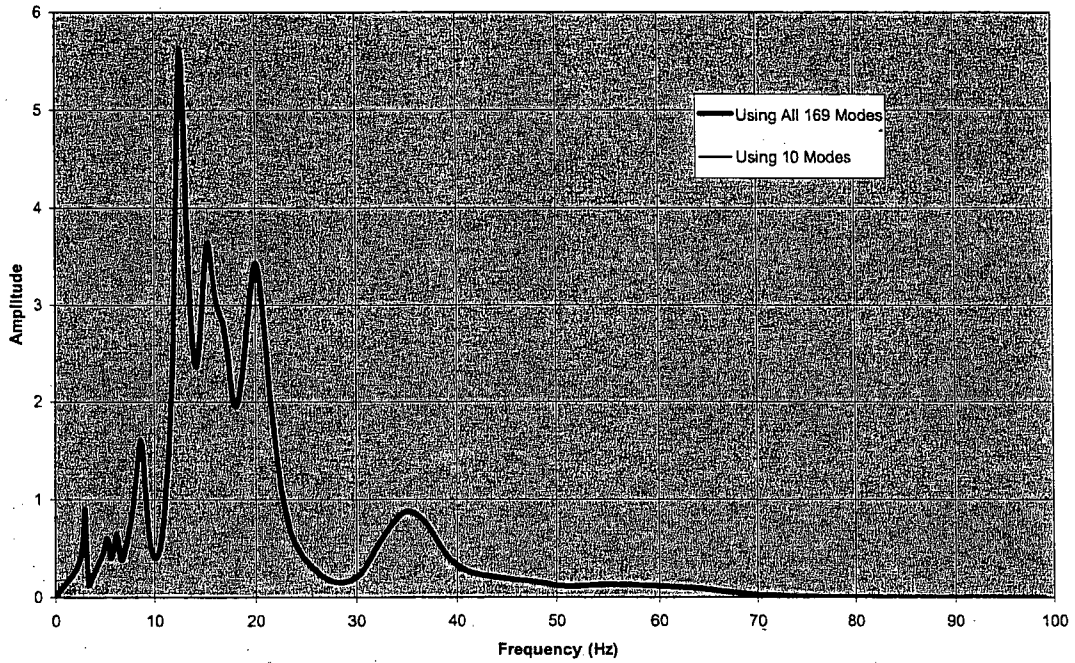


Figure 6.43

**Effects of Using Limited Spatial Modal Solutions for Incoherent Motion Analysis
Z-X Transfer Functions at Node 229 (CIS Outrigger), AP1000 Outrigger Model.**

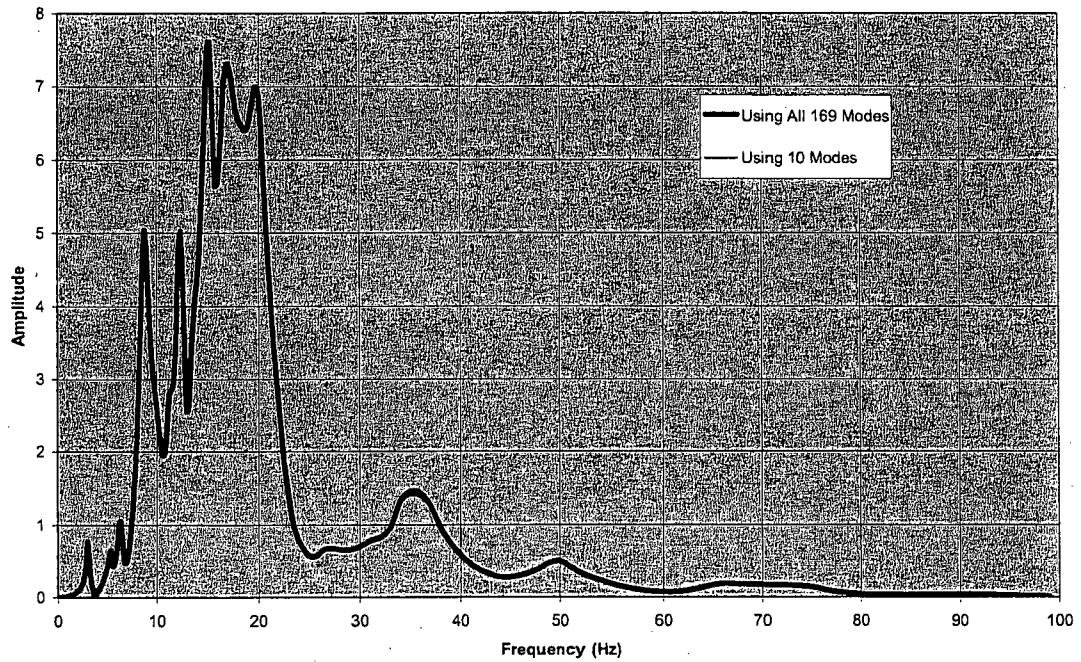
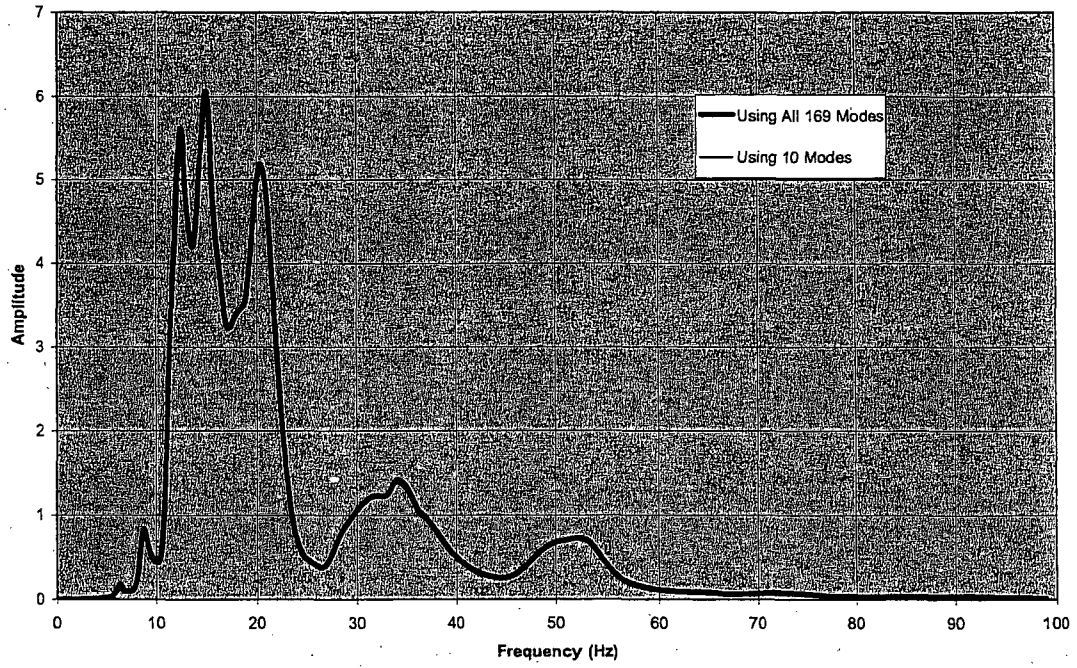


Figure 6.44

**Effects of Using Limited Spatial Modal Solutions for Incoherent Motion Analysis
Z-Y Transfer Functions at Node 229 (CIS Outrigger), AP1000 Outrigger Model.**



7. Summary and Conclusion

The document presented herein summarizes the theoretical formulation and implementation of the SRSS method for analyzing ground motion incoherency effects in SASSI2000. A brief discussion of the two incoherency models is presented and the formulation that describes the reason for adoption and applicability of the SRSS method is fully described. A summary of the verification examples verifying the solutions with available published solutions and the solutions obtained from the computer program CLASSI is presented. Sensitivity analyses are performed for all verification examples on effects of using limited spatial modal solutions. Results of the sensitivity analyses indicate that for practical purposes, using 10 spatial modes in the SSI analysis shall be adequate in capturing the major effects of incoherent ground motions.

Based on the derivation and verification presented in this document, it is concluded that the SRSS method for analyzing the ground motion incoherency effects implemented in SASSI2000 is an accurate method and can be used for design.

8. References

Abrahamson, N. (2006). "Spatial Coherency for Soil-Structure Interaction, EPRI, Final report 1014101, Palo Alto, CA, August (draft)

Abrahamson, N. (2007). "Hard Rock Coherency for Soil-Structure Interaction Based on the Pinyon Flat Data, April.

Lysmer, J., Ostadan, F., Chin, C. (1999) "SASSI2000", Geotechnical Engineering Division, Civil Engineering Department, University of California, Berkeley, CA 94720

Luco, J. E., and Mita, A. (1987) "Response of Circular Foundation to Spatially Random Ground Motion," *ASCE Journal of Engineering Mechanics*, Vol. 113, No. 1, pp. 1-15, January.

Mita, A. and Luco J.E. (1986): "Response of Structures to Spatially Random Ground Motion," Proceedings of the Third U.S. Conference on Earthquake Engineering, Charleston, South Carolina.

EPRI (2007), Final Report: "Validation of CLASSI and SASSI to Treat Seismic Wave Incoherence in SSI Analysis of Nuclear Power Plant Structures, August .

ATTACHMENT A

SUBSTRUCTURING METHODS OF SASSI2000

(Chapter 2 of SASSI2000 Theoretical Manual)

A.1 SUBSTRUCTURING METHODS OF SSI ANALYSIS

The soil-structure interaction problem is most conveniently analyzed using a substructuring approach. In this approach, the linear soil-structure interaction problem is subdivided into a series of simpler sub-problems. Each sub-problem is solved separately and the results are combined in the final step of the analysis to provide the complete solution using the principle of superposition.

For the case of structures with surface foundations for which the structure and the foundation interface boundary is on the surface of the foundation medium, the substructuring method is relatively simple and many solution techniques are available. For structures with embedded foundations, the substructuring method becomes considerably more complicated. Conceptually, these methods can be classified into four types depending on how the interaction at the soil and structure interface degrees-of-freedom is handled. These four types are: 1) the rigid boundary method, 2) the flexible boundary methods, 3) the flexible volume method, and 4) the substructure subtraction method. The seismic SSI sub-problems that these four types of substructuring methods are required to solve to obtain the final solution are compared in Fig. A.1-1. As shown in this figure, the solution for the site response problem is required by all four methods. This is, therefore, common to all methods. The analysis of the structural response problem is also required and involves essentially the same effort for all methods. The necessity and effort required for solving the scattering and impedance problems, however, differ significantly among the different methods. For the rigid-boundary and the flexible-boundary methods, two explicit analyses are required separately for solving the scattering and impedance problems. On the other hand, the flexible volume method and the substructure subtraction method, because of the unique substructuring technique (see Sections A.2 and A.3), require only one impedance analysis and the scattering analysis is eliminated. Furthermore, the substructuring in the subtraction method often requires a much smaller impedance analysis than the flexible volume method. The SASSI computer program adopts both the flexible volume method and the substructure subtraction method of substructuring.

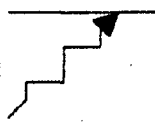
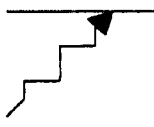
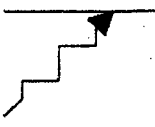
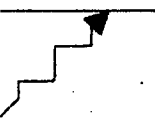
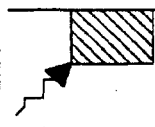
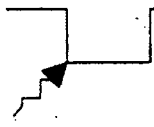
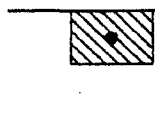
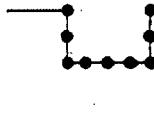
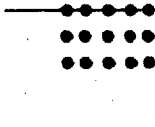
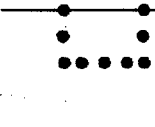
Method Analysis	Rigid Boundary	Flexible Boundary	Flexible Volume	Subtraction
Site Response Analysis (a)				
Scattering Analysis (b)			None	None
Impedance Analysis (c)				
Structural Response Analysis (d)	Standard	Standard +	Standard +	Standard +

Figure A.1-1. Summary of Substructuring Methods

A.2 THE FLEXIBLE VOLUME METHOD

The flexible volume substructuring method is based on the concept of partitioning the total soil-structure system as shown in Fig. A.2-1a into three substructure systems as shown in Figs. A.2-1b, A.2-1c and A.2-1d. The substructure I consists of the free-field site, the substructure II consists of the excavated soil volume, and the substructure III consists of the structure, of which the foundation replaces the excavated soil volume. The substructures I, II and III, when combined together, form the original SSI system shown in Fig. A.2-1a. The flexible volume method presumes that the free-field site and the excavated soil volume interact both at the boundary of the excavated soil volume and within its body, in addition to interaction between the substructures at the boundary of the foundation of the structure. The theory and formulation that develop in the following sections are equally applicable to two- and three-dimensional SSI problems.

The equations of motion for the SSI substructures shown in Figs. A.2-1b, A.2-1c and A.2-1d can be written in the following matrix form:

$$[M] \{\hat{U}\} + [K] \{\hat{U}\} = \{\hat{Q}\} \quad (\text{A.2-1})$$

where $[M]$ and $[K]$ are the total mass and stiffness matrices, respectively. $\{\hat{U}\}$

is the vector of total nodal point displacements and $\{\hat{Q}\}$ are the forces due to applied external dynamic forces or seismic excitations.

For the harmonic excitation at frequency ω , the load and the displacement vectors can be written as

$$\{\hat{Q}\} = \{Q\} \exp(i\omega t) \quad (\text{A.2-2})$$

And

$$\{\hat{U}\} = \{U\} \exp(i\omega t) \quad (\text{A.2-3})$$

where $\{Q\}$ and $\{U\}$ are the complex force and displacement vectors at frequency ω . Hence, for each frequency, the equations of motion take the form

$$[C] \{U\} = \{Q\} \quad (\text{A.2-4})$$

where $[C]$ is a complex frequency-dependent dynamic stiffness matrix:

$$[C] = [K] - \omega^2[M] \quad (\text{A.2.5})$$

Using the following subscripts, which refer to degrees of freedom associated with different nodes (see Fig. A.2-1):

<u>Subscript</u>	<u>Nodes</u>
b	the boundary of the total system
i	at the boundary between the soil and the structure
w	within the excavated soil volume
g	at the remaining part of the free-field site
s	at the remaining part of the structure
f	combination of i and w nodes

The equation of motion for the system is partitioned as follows:

$$\begin{bmatrix} C_{ii}^{III} - C_{ii}^{II} + X_{ii} & -C_{iw}^{II} + X_{iw} & C_{is}^{III} \\ -C_{wi}^{II} + X_{wi} & -C_{ww}^{II} + X_{ww} & 0 \\ C_{si}^{III} & 0 & C_{ss}^{III} \end{bmatrix} \begin{Bmatrix} U_i \\ U_w \\ U_s \end{Bmatrix} = \begin{Bmatrix} X_{ii} U'_i + X_{iw} U'_w \\ X_{wi} U'_i + X_{ww} U'_w \\ 0 \end{Bmatrix} \quad (\text{A.2-6})$$

where superscripts, I, II and III, refer to the three substructures. The complex frequency-dependent dynamic stiffness matrix on the left of Equation (A.2-6) simply indicate the stated partitioning according to which the stiffness and mass of the excavated soil volume are subtracted from the dynamic stiffness of the free-

field site and the structure. The frequency-dependent matrix, $\begin{bmatrix} X_{ii} & X_{iw} \\ X_{wi} & X_{ww} \end{bmatrix}$ or

$\begin{bmatrix} X_{ff} \end{bmatrix}$, is called the impedance matrix, which is obtained from the model in

substructure I using the point load solutions. The vector, $\begin{Bmatrix} U'_i \\ U'_w \end{Bmatrix}$ or $\begin{Bmatrix} U'_f \end{Bmatrix}$,

computed from the free-field motion for the interacting nodes shown in substructure I. The motion is a function of prescribed wave field in the free-field. The methods for solving the site response problem for body and surface waves are described in Chapter 3. Degrees of freedom associated with nodes i and w are considered interacting and included in the impedance analysis and in the load vector in Equation (A.2-6).

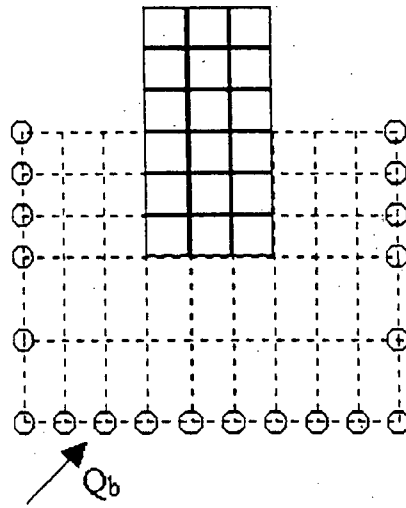
If the source of excitation is applied dynamic loading within the model, as in the case of foundation vibrations, impact loads, and wind loads, the free-field motions

$\begin{Bmatrix} U'_i \\ U'_w \end{Bmatrix}$ vanish and Equation (A.2-6) can be written as

$$\begin{bmatrix} C_{ii}^{III} - C_{ii}^{II} + X_{ii} & -C_{iw}^{II} + X_{iw} & C_{is}^{III} \\ -C_{wi}^{II} + X_{wi} & -C_{ww}^{II} + X_{ww} & 0 \\ C_{si}^{III} & 0 & C_{ss}^{III} \end{bmatrix} \begin{Bmatrix} U_i \\ U_w \\ U_s \end{Bmatrix} = \begin{Bmatrix} P_i \\ 0 \\ P_s \end{Bmatrix} \quad (\text{A.2-7})$$

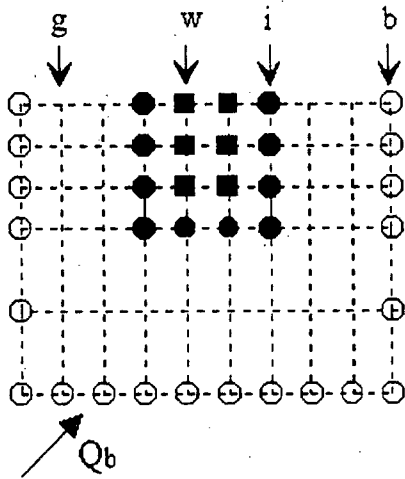
where the load vector has non-zero terms only where external loads are applied.

Seismic and external loads can, in principle, be considered together by simply adding the external loads $\{P\}$ to the load vector in Equation (A.2-6). This method is not used in SASSI, since in practice; the seismic excitations and the external loads are seldom considered simultaneously.

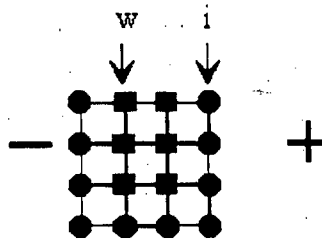


(a) Total System

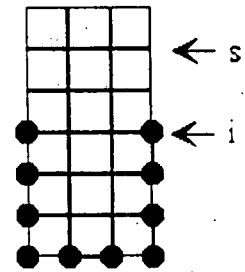
||



(b)
Substructure I
Free-Field Site



(c)
Substructure II
Excavated Soil Volume



(d)
Substructure III
Structure

Figure A.2-1. Sub-structuring in the Flexible Volume Method

A.3 THE SUBSTRUCTURE SUBTRACTION METHOD

The substructure subtraction method is basically based on the same substructuring concept as the flexible volume method. The subtraction method partitions the total soil-structure system as shown in Fig. A.3-1a into three substructure systems as shown in Figs. A.3-1b, A.3-1c and A.3-1d. The substructure I consists of the free-field site, the substructure II consists of the excavated soil volume, and the substructure III consists of the structure. The substructures I, II and III, when combined together, form the original SSI system shown in Fig. A.3-1a. However, the subtraction method recognizes that soil-structure interaction occurs only at the common boundary of the substructures, that is, at the boundary of the foundation of the structure. This often leads to a smaller impedance analysis than the flexible volume method. The theory and formulation that develop in the following sections are equally applicable to two- and three-dimensional SSI problems.

The equations of motion for the SSI substructures shown in Figs. A.3-1b, A.3-1c and A.3-1d can be written in the following matrix form as in the flexible volume method:

$$[M] \{ \hat{U} \} + [K] \{ \hat{U} \} = \{ \hat{Q} \} \quad (A.3-1)$$

where $[M]$ and $[K]$ are the total mass and stiffness matrices, respectively. $\{ \hat{U} \}$ is the vector of total nodal point displacements and $\{ \hat{Q} \}$ are the forces due to applied external dynamic forces or seismic excitations.

For the harmonic excitation at frequency ω , the equations of motion can take the form as discussed in Section A.2:

$$[C] \{ U \} = \{ Q \} \quad (A.3-2)$$

where $\{ Q \}$, $\{ U \}$ and $[C]$ are the complex force vector, the complex displacement vector and the complex frequency-dependent dynamic stiffness matrix, respectively.

Use the same subscripts as in the flexible volume method to refer to degrees of freedom associated with different nodes (see Fig. A.3-1):

<u>Subscript</u>	<u>Nodes</u>
b	the boundary of the total system
i	at the boundary between the ground and the structure
w	within the excavated soil volume
g	at the remaining part of the free-field site
s	at the remaining part of the structure
f	same as i nodes

The equation of motion for the system is partitioned as follows in the subtraction method:

$$\begin{bmatrix} C_{ii}^{III} - C_{ii}^{II} + X_{ii} & -C_{iw}^{II} & C_{is}^{III} \\ -C_{wi}^{II} & -C_{ww}^{II} & 0 \\ C_{si}^{III} & 0 & C_{ss}^{III} \end{bmatrix} \begin{Bmatrix} U_i \\ U_w \\ U_s \end{Bmatrix} = \begin{Bmatrix} X_{ii} U_i' \\ 0 \\ 0 \end{Bmatrix} \quad (A.3-3)$$

where superscripts, I, II and III, refer to the three substructures. The complex frequency-dependent dynamic stiffness matrix on the left of Equation (A.3-3) indicates the stated partitioning according to which the stiffness and mass of the excavated soil are subtracted from the dynamic stiffness of the free-field site and the structure. Compared to Equation (A.2-6) in Section A.2 for the flexible volume method, this complex dynamic stiffness is much simpler because only the degrees of freedom associated with nodes i are considered interacting. This also leads to an impedance analysis involving less number of degrees of freedom and therefore a smaller impedance matrix, $[X_{ii}]$ or $[X_{ff}]$, which will be described in Chapter 4. For the same reason, only the free-field motions at the degrees of freedom associated with nodes i, $\{U_i'\}$ or $\{U_f'\}$, computed from the site response analysis are part of the load vector in Equation (A.3-3). The methods for solving the site response problem for body and surface waves are described in Chapter 3.

If the source of excitation is applied dynamic loading within the model, as in the case of foundation vibrations, impact loads, and wind loads, the free-field motions $\{U_i'\}$ vanish and Equation (A.3-3) can be written as

$$\begin{bmatrix} C_{ii}^{III} - C_{ii}^{II} + X_{ii} & -C_{iw}^{II} & C_{is}^{III} \\ -C_{wi}^{II} & -C_{ww}^{II} & 0 \\ C_{si}^{III} & 0 & C_{ss}^{III} \end{bmatrix} \begin{Bmatrix} U_i \\ U_w \\ U_s \end{Bmatrix} = \begin{Bmatrix} P_i \\ 0 \\ P_s \end{Bmatrix} \quad (\text{A.3-4})$$

where the load vector has non-zero terms only where external loads are applied.

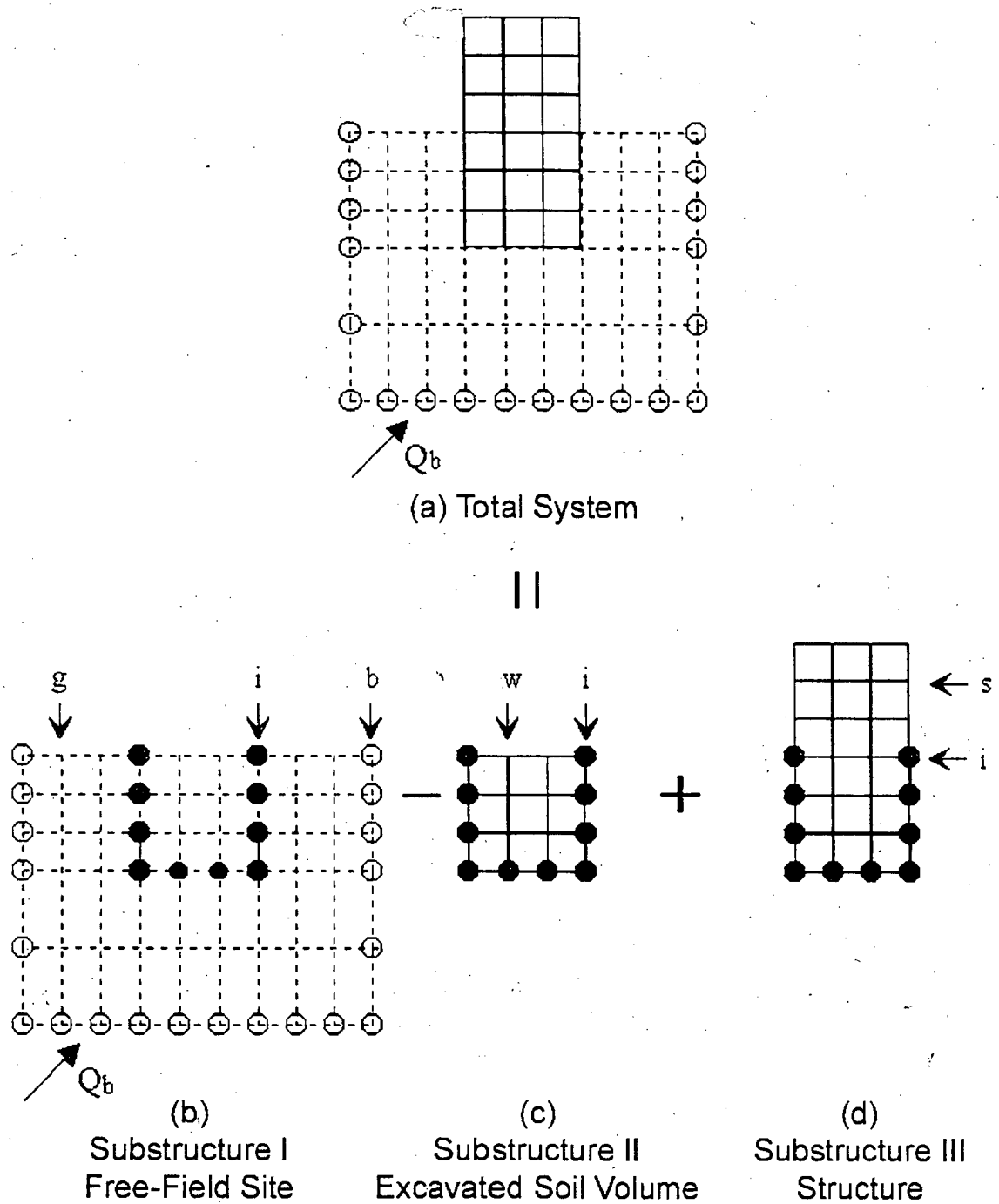


Figure A.3-1. Sub-structuring in the Substructure Subtraction Method